



This is a repository copy of *Autophagy in osteoblasts is involved in mineralization and bone homeostasis*.

White Rose Research Online URL for this paper:  
<http://eprints.whiterose.ac.uk/98162/>

Version: Accepted Version

---

**Article:**

Nollet, M., Santucci-Darmanin, S., Breuil, V. et al. (19 more authors) (2014) Autophagy in osteoblasts is involved in mineralization and bone homeostasis. *Autophagy*, 10 (11). pp. 1965-1977. ISSN 1554-8627

<https://doi.org/10.4161/auto.36182>

---

**Reuse**

Unless indicated otherwise, fulltext items are protected by copyright with all rights reserved. The copyright exception in section 29 of the Copyright, Designs and Patents Act 1988 allows the making of a single copy solely for the purpose of non-commercial research or private study within the limits of fair dealing. The publisher or other rights-holder may allow further reproduction and re-use of this version - refer to the White Rose Research Online record for this item. Where records identify the publisher as the copyright holder, users can verify any specific terms of use on the publisher's website.

**Takedown**

If you consider content in White Rose Research Online to be in breach of UK law, please notify us by emailing [eprints@whiterose.ac.uk](mailto:eprints@whiterose.ac.uk) including the URL of the record and the reason for the withdrawal request.



[eprints@whiterose.ac.uk](mailto:eprints@whiterose.ac.uk)  
<https://eprints.whiterose.ac.uk/>

# Autophagy in Osteoblasts is involved in Mineralization and Bone

## Homeostasis

Marie Nollet<sup>1</sup>, Sabine Santucci-Darmanin<sup>1</sup>, Véronique Breuil<sup>1,2</sup>, Rasha Al-Sahlane<sup>1</sup>,  
Chantal Cros<sup>1</sup>, Majlinda Topi<sup>1</sup>, David Momier<sup>1</sup>, Michel Samson<sup>1</sup>, Sophie Pagnotta<sup>3</sup>,  
Laurence Cailleateau<sup>4</sup>, Séverine Battaglia<sup>5</sup>, Delphine Farlay<sup>6</sup>, Romain Dacquin<sup>7</sup>, Nicolas  
Barois<sup>8</sup>, Pierre Jurdic<sup>7</sup>, Georges Boivin<sup>6</sup>, Dominique Heymann<sup>5</sup>, Franck Lafont<sup>9</sup>, Shi Shou  
Lu<sup>10</sup>, David W. Dempster<sup>10</sup>, Georges F. Carle<sup>1</sup> and Valérie Pierrefite-Carle<sup>1</sup>.

<sup>1</sup> UMR E-4320 MATOs CEA/iBEB/SBTN-CAL, Université Nice Sophia Antipolis, Faculté de Médecine Nice, France ; <sup>2</sup> Service de Rhumatologie, CHU de Nice, Nice, France; <sup>3</sup> Centre Commun de Microscopie Appliquée, Université Nice Sophia Antipolis, Nice, France ; <sup>4</sup> Plateforme Imagerie IRCAN, Faculté de Médecine, Université Nice Sophia Antipolis, Nice, France; <sup>5</sup> INSERM UMR 957 Université de Nantes, Equipe labellisée Ligue Nationale Contre le Cancer 2012, Nantes, France; <sup>6</sup> INSERM UMR 1033, Université de Lyon, France; <sup>7</sup> Institut de Génomique Fonctionnelle de Lyon, Université de Lyon, CNRS, Ecole Normale Supérieure de Lyon, Lyon, France; <sup>8</sup> Plate-forme BICeL-IFR142, Institut Pasteur de Lille, Lille, France; <sup>9</sup> INSERM U1019 - CNRS UMR 8204, Institut Pasteur de Lille - Univ Lille Nord de France, Lille, France; <sup>10</sup> Regional Bone Center, Helen Hayes Hospital, West Haverstraw, New York, USA.

Short title: Autophagy involvement in osteoblast function

Keywords: autophagy; osteoblast; mineralization; bone remodeling

Conflict of interest: none

Financial interest disclosure: none

**Correspondence to:** Dr Valérie Pierrefite-Carle, PhD, MATOs UMR E4320 CEA/CAL/UNS,

Faculté de Médecine, Avenue de Valombrose, 06107 Nice cédex 2, France.

Phone : +33 4 93 37 77 06, Fax : +33 4 93 53 30 71, Email: [pierrefi@unice.fr](mailto:pierrefi@unice.fr)

## Abstract

Bone remodeling is a tightly controlled mechanism in which osteoblasts (OB), the cells responsible for bone formation, osteoclasts (OC), the cells specialized for bone resorption, and osteocytes, the multifunctional mechanosensing cells embedded in the bone matrix, are the main actors. Increase oxidative stress in OB, the cells producing and mineralizing bone matrix, has been associated with osteoporosis development but the role of autophagy in OB has not yet been addressed. This is the goal of the present study.

We first show that the autophagic process is induced in OB during mineralization. Then, using knockdown of autophagy-essential genes and OB-specific autophagy-deficient mice, we demonstrate that autophagy deficiency reduces mineralization capacity. Moreover, our data suggest that autophagic vacuoles could be used as vehicles in OB to secrete hydroxyapatite crystals. In addition, autophagy-deficient OB exhibit increased oxidative stress and receptor activator of NF- $\kappa$ B (RANKL) secretion, favoring generation of osteoclasts (OC), the cells specialized in bone resorption. *In vivo*, we observed a 50% reduction in trabecular bone mass in OB-specific autophagy-deficient mice.

Taken together, our results show for the first time that autophagy in OB is involved both in the mineralization process and in bone homeostasis. These findings are of importance for mineralized tissues which extends from corals to vertebrates and uncovers new therapeutics targets for calcified tissue related metabolic pathologies.

## Introduction

Bone remodeling is a tightly controlled mechanism in which osteoblasts (OB), the cells responsible for bone formation, osteoclasts (OC), the cells specialized for bone resorption, and osteocytes, the multifunctional mechanosensing cells embedded in the bone matrix, are the main actors.<sup>1</sup> The remodeling process is highly active throughout the life and perturbation of this process can lead to many pathologies including osteoporosis. This pathology, due to an imbalance favoring bone resorption over formation, is characterized by increased OB apoptosis as well as an enhanced OC number and activity.<sup>2</sup> Although age-related estrogen deficiency has long been considered to be the major cause of osteoporosis, the oxidative stress increase associated with aging is now also proposed to be a key factor leading to this pathology.<sup>3</sup>

Autophagy is the major catabolic process of eukaryotic cells that degrades and recycles damaged macromolecules and organelles.<sup>4,5</sup> During this process, the cytoplasmic material targeted to degradation is delivered to lysosomes upon sequestration within double-membraned vesicles that are called autophagosomes. Autophagosomes and their contents are cleared upon fusing with late endosomes or lysosomes, and products of these catabolic reactions can then re-enter anabolic and/or bioenergetic metabolisms.<sup>4,6</sup> Autophagy occurs at low level in all cells to ensure the homeostatic turnover of long-lived proteins and organelles<sup>7</sup> and is upregulated under stressful conditions.<sup>8</sup>

In the present work, we address the role of autophagy in OB based on several considerations. First, regulation of bone cell survival/apoptosis is a crucial mechanism in the control of the

OB to OC cell ratio, and therefore, in bone remodeling. As autophagy is a cell survival mechanism, its role in the OB could potentially influence the balance between bone formation and bone resorption. Second, several autophagy-inducers in non-osteoblastic cells, such as calcium, vitamin D3 and resveratrol are known to be beneficial to bone health.<sup>9,10,11</sup> In addition, recent studies demonstrated a link between autophagy and some secretion process<sup>12,13</sup> and one of the main OB functions is extracellular matrix production. Furthermore, oxidative stress, which can be alleviated by autophagy, appears to be a key factor in the major age-related bone disease, osteoporosis.<sup>3</sup> Finally, a link between autophagy genes and human height and osteoporosis has been recently highlighted in human genome-wide association data.<sup>14,15</sup>

Here we provide evidence for a direct role of autophagy in the OB intracellular mineralization process, as well as an indirect effect on bone remodeling through the stimulation of osteoclastogenesis. Indeed, autophagy appears to be highly induced during mineralization in OB and its inhibition leads to a drastic drop in the efficiency of this central OB function in vitro. Further examination of primary autophagy-deficient OB displayed elevated oxidative stress level associated with a ten fold increased receptor activator of NF- $\kappa$ B (RANKL) secretion thus driving sustained osteoclastogenesis. Finally, OB specific impairment of autophagy in vivo leads to a significant loss in trabecular bone in nine month-old female mice.

## Results

### Autophagy is increased during mineralization in vitro

To address the role of autophagy in OB, we first analyzed the autophagic process during the 6 days course of mineralization in the UMR-106 osteoblastic cell line. Upon autophagy induction, the essential autophagy protein microtubule-associated protein 1 light chain 3 protein (LC3-I) becomes lipidated (LC3-II) and inserts into the autophagosome membrane.

<sup>16,17,18</sup> One of the widely used methods to detect autophagy is thus based on the quantification of the LC3-II protein by western blot. As shown in Figure 1A, we observed an increase in the steady-state levels of the LC3-II protein during the course of mineralization, suggesting an increase in the number of autophagosomes. An increase in LC3-II level can be due either to an increased autophagosome formation or a block in autophagosome maturation. To differentiate between these two possibilities, we clamped the LC3-II autophagosome degradation by the use of the lysosomal proton pump inhibitor Bafilomycin-A<sub>1</sub>.<sup>19</sup> In Bafilomycin-A<sub>1</sub>-treated cells, LC3-II levels were further increased at each time point, suggesting that mineralization is associated with enhanced autophagosome formation. After transfection of a GFP-LC3 construct, autophagosome formation can also be scored by immunofluorescence microscopy as a transition of LC3 from its diffuse cytosolic appearance to a membrane-associated, punctate intracellular distribution.<sup>20</sup> In the UMR-106 cell line stably expressing the GFP-LC3 plasmid, the LC3 protein mainly exhibited a diffuse localization at day 3, before the emergence of mineralization foci (Fig.1B). However at day 5, we observed a global decrease of the GFP signal, associated with the appearance of autophagic cells, especially in the vicinity of the mineralization foci, confirming autophagy

induction during mineralization. We then analyzed by transmission electron microscopy the autophagic vesicles present in mineralizing UMR-106 cells. As shown in Figure 1C, we observed the presence of double-membraned autophagic vesicles containing needle-like structures resembling crystals that seemed to be released in the extracellular medium. We confirmed the crystalline nature of these structures by high-resolution transmission electron microscopy (Fig.1D). X-ray microanalysis revealed calcium ( $\text{CaK}\alpha$ ), phosphorus ( $\text{PK}\alpha$ ) and oxygen ( $\text{OK}\alpha$ ) elements as the main components of these needle-like structures (Fig.1E). Selected area electron diffraction patterns were measured to obtain the corresponding interplanar distances. The bone mineral hydroxyapatite was identified by diffractogram analysis, which showed the presence of two diffraction rings matching the characteristic spacings for hydroxyapatite (3.45 and 2.81 Å) (Fig.1F). Taken together, these data suggest that the autophagic vacuoles could serve as vehicles for mineralization crystals. In agreement with this hypothesis, autophagosomes moving to the plasma membrane can be observed by confocal time-lapse video of mineralizing UMR GFP-LC3 cells (Movie 1).

We then analyzed the autophagic process during mineralization in mouse primary OB isolated from calvariae. Between day 5 and day 12, we observed an 6.6-fold increase in the steady-state levels of the LC3-II protein (Fig.2A), suggesting an increase in the number of autophagosomes during mineralization. Bafilomycin- $\text{A}_1$  treatment caused a 13.7 and 2.5-fold increase in LC3-II levels at day 5 and 12 respectively, indicating that autophagosome formation is enhanced during mineralization, particularly in the early phase. As in the UMR-106 cell line, analysis by transmission electron microscopy of these primary mouse OB during mineralization showed the presence of autophagic vacuoles containing crystal-like structures (Fig. 2B and C) and X-ray microanalysis demonstrated the presence of calcium and phosphorus (Fig.1D) present as hydroxyapatite crystals (Fig.1E).

### **The autophagy proteins Atg7 and Beclin-1 are required for mineralization in an osteoblastic cell line**

To investigate the potential direct relationship between autophagy and mineralization, we then used siRNAs targeting two proteins involved in autophagy during mineralization of the UMR-106 cell line. Knockdown of *Atg7*, which is involved in phagophore elongation and LC3 lipidation,<sup>21</sup> induced a significant decrease in mineralizing nodules (Fig. 3 A-C). To confirm these results, we then inhibited the expression of *Beclin 1 (BECN1)* which is involved in the initiation step of the autophagic process and regulates both the formation and maturation of autophagosomes.<sup>22,23,24</sup> Similarly, BECN1 knockdown significantly reduced mineralization capacity (Fig.3 D-F). These results thus demonstrate involvement of autophagy in the OB mineralization process.

### **Atg5 deficiency in primary osteoblasts reduces mineralization capacity ex vivo and increases OC number**

To assess the physiological role of autophagy in primary OB, we bred *Atg5<sup>flox-flox</sup>* mice<sup>25</sup> to those expressing Cre recombinase under the control of the osteoblastic type 1a collagen (Col1A) promoter.<sup>26</sup> Deletion of the *Atg5* gene in osteoblasts was checked by PCR on cortical bone genomic DNA (supplementary Fig. S1 A-B). This *Atg5* gene deletion led to a 75% reduction in the amount of LC3-II protein in cortical bone of mutant mice compared to their control littermates indicating a decreased autophagic activity (supplementary Fig. S1 C).

We then cultured bone explants from the calvariae of *Atg5<sup>flox-flox</sup> Col1A-Cre-* and *Atg5<sup>flox-flox</sup> Col1A-Cre+* mice and analyzed mineralization capacity in these cultures. As shown in Figure 4, we observed a reduced mineralization in bone explant cultures derived from mutant mice compared to the one observed in cultures from control mice. In these experiments, cultures from mutant mice exhibited a high number of large multinucleated cells which were positive for tartrate-resistant alkaline phosphatase (TRAP) staining, suggesting the presence of osteoclast-like cells (Fig. 5 A-B). Some osteoclast-like cells were also observed in cultures from control mice but were less numerous. As RANKL represents one of the major cytokines involved in osteoclastogenesis, we then measured secreted RANKL levels in cultures from control and mutant mice. Enzyme-linked immunosorbent assays showed that the concentration of RANKL increased 9.7-fold in cultures from mutant mice compared to that observed in cultures from control mice ( $p < 0.05$ ) (Fig. 5C). Increased RANKL production was described to be associated with increased oxidative stress in osteoblasts.<sup>27,28,29</sup> Therefore, we next analyzed oxidative stress in cultures from control and mutant mice and observed a significant increase in reactive oxygen species (ROS) in cultures from mutant mice (Fig.5D). Finally, we analyzed the expression of different osteoblastic markers in calvariae from control and mutant mice. As shown in Figure 5E, a significant increase in runt-related transcription factor 2 (Runx2) and osteopontin (OPN) expression was observed in mutant calvarial bones compared to controls, although the collagen mRNA levels remained unchanged.

### **Atg5 deficiency in osteoblasts results in decreased bone volume in vivo**

To determine the *in vivo* consequences of *Atg5* loss in osteoblasts, we characterized the

skeletal phenotype of *Atg5<sup>flox-flox</sup> Col1A-Cre+* mice. Histomorphometric analysis of femur of nine-month-old female and male mice confirmed the deleterious effect of the *Atg5* inactivation on bone mass by revealing a reduction in trabecular bone volume associated with decreased trabecular width and number (Fig. 6 A-D and supplementary Fig. S2). This effect was more pronounced in females compared to male mice. We also observed a significant reduction in OB perimeter and a trend towards an increase in OC perimeter in the mutant mice of both sexes (Fig. 6 E-F), resulting in a significant decrease of the OB to OC ratio in mutant female and male mice compared to their control littermates (44 % and 64 % decrease in OB to OC ratio respectively in mutant female and male mice compared to controls) (Fig. 6G). Finally, mineral apposition rate (MAR) was evaluated, showing a 50% decrease in mutant compared to control 9-month old mice ( $0,58 \pm 0,05$  compared to  $1,14 \pm 0,19$  microns/day). Microcomputerized tomography confirmed these results with a significantly decreased bone volume, intersection surface, trabecular number and increased trabecular spacing in females (Table 1 and Fig. 7). Although not statistically significant, a similar trend was observed in males.

## Discussion

The role of autophagy in bone cells was recently highlighted by several studies.<sup>30</sup> Autophagy was first shown to be a major survival mechanism of the long-lived osteocytes in stressful environments.<sup>31,32,33</sup> Recent work by Onal M. *et al.* reported that autophagy suppression in osteocytes results in a reduced bone volume of six-month old mice associated with an overall reduction in OB and OC numbers.<sup>34</sup> The study of Whitehouse *et al.*,<sup>35</sup> then demonstrated that genetic truncation of the selective autophagic receptor Nbr1 in a murine model leads to increased osteoblast differentiation and activity *in vivo*. In OC, proteins essential for autophagy were shown to be key factors for ruffled border formation, secretory function, and bone resorption *in vitro* and *in vivo*.<sup>36</sup> Finally, very recent work by Pantovic *et al.*<sup>37</sup> demonstrated that genetic or pharmacological autophagy inhibition suppressed mesenchymal stem cell differentiation to OB. In the present work, we addressed for the first time the role of autophagy in OB function.

One of the main roles of OB is to produce and mineralize bone matrix. Mineralization is a complex and incompletely understood process involving several concurrently redundant mechanisms.<sup>38</sup> Mineral formation is proposed to be initiated inside vesicles, either after their secretion, as in matrix vesicles<sup>39,40</sup> or before their secretion, inside the cell.<sup>41,42</sup> This last process called intracellular mineralization is initiated by the generation of mineral-containing needle-shaped structures that form aggregates. These aggregates are then included in vesicles of an unknown nature that were observed to move to the cell membrane where exocytosis occurs.<sup>41,43</sup> [In this report, we show the presence of mineral organized as needle-like](#)

structures mainly within autophagic vesicles. Based on the Ca/P ratio, this mineral appears to be immature. As chemical fixation can cause the artifactual crystallization of calcium phosphate<sup>44</sup>, we cannot completely rule out the possibility that the mineral is in fact present under an amorphous state. However, the absence of such needle-like structures within mitochondria tend to favor the crystalline nature of these aggregates.

Our results indicate that mineralization is associated with an autophagy induction and that autophagy inhibition results in a decreased mineralization capacity in OB cells. In addition, transmission electron microscopy and confocal time-lapse live cell imaging suggest that autophagic vacuoles could serve as vehicles to secrete hydroxyapatite crystals into the extracellular space. In addition to its role in physiological conditions, the intracellular mineralization process is also involved in pathological calcification of soft tissues which is associated with serious clinical consequences.<sup>45</sup> In this regard, mineralized structures within autophagic vacuoles have been observed in kidney epithelial cells cultured under mineralizing conditions.<sup>45</sup>

Recent publications provide evidence that autophagy is involved in some secretion mechanisms.<sup>12,13</sup> In particular, although the classical fate of autophagosomes is fusion with lysosomes and degradation of their contents, several studies have demonstrated an exocytosis of autophagic vacuole content within the extracellular medium.<sup>46-53</sup> This autophagy-based exocytic process has been described for the unconventional secretion of proteins devoid of signal peptide such as Acb1<sup>46,47</sup> and IL-1 proteins.<sup>48</sup> In addition to the secretion of these cytosolic proteins, exocytosis of autophagic vacuole content was also observed in stressed cells,<sup>50,51</sup> to be involved in cellular remodeling during the final maturation of reticulocytes<sup>52</sup>

and in elimination of actin-rich ordered paracrystalline filament arrays called Hirano bodies.

53

In addition to a direct effect on mineralization, autophagy deficiency in OB also alters the cross-talk with OC and favor the formation of the latter due to an increase in RANKL secretion. While autophagy suppression in osteocytes results in a low rate bone remodeling associated with reduced OB and OC numbers,<sup>34</sup> autophagy deficiency in OB leads to an osteoporotic-like phenotype, with an enhanced osteoclastogenesis. Several studies demonstrate that increased oxidative stress in OB leads to increased RANKL production.

<sup>27-29</sup> Moreover, autophagy deficiency is known to be associated with increased oxidative stress, partly due to the accumulation of damaged mitochondria.<sup>54</sup> We also observed an increased oxidative stress in mutant bone explant cultures compared to control. A trend towards an increase in OC number in cultures from mutant mice was also observed *in vivo* by histomorphometric analysis and was associated with a reduced OB perimeter, which is consistent with previous studies linking increased oxidative stress with decreased OB number.

<sup>55-57</sup> We also determined that Runx2 and OPN were significantly increased at the transcriptional level in calvariae from mutant mice compared to controls. Runx2 is the master transcription factor in OB, the expression of which is absolutely required for bone formation and function.<sup>58,59</sup> However, Runx2 is also known to modulate prosurvival mechanisms

associated with transcription of genes such as Bcl-2 or OPN,<sup>60-63</sup> the latter being also known as a stress-induced factor.<sup>64</sup> In addition, endoplasmic reticulum stress, which is often

associated with autophagy deficiency,<sup>65</sup> was shown to induce apoptosis and transcriptional

upregulation of Runx2.<sup>66</sup>

Finally, we observed that autophagy deficiency in OB results in decreased bone volume in 9-month old mice. In vivo, it is likely that a defect in intracellular mineralization process due to autophagy deficiency in OB can be compensated in young animals by other cooperative and redundant mechanisms. The significantly decreased bone volume observed in aged animals suggest that increased oxidative stress associated with aging could constitute the major mechanism leading to bone loss upon OB autophagy deficiency. A significant effect was mostly observed in female mice, although males exhibit a similar tendency. Age- and gender-dependent bone phenotypes in mice with genetic alterations in different pathways have previously been described. For example, genetic manipulation of *Lef1*, *GSK3 $\beta$* , *sFRP1* or *Cathepsin K* led to a female-preferential bone phenotype.<sup>67-69</sup> In addition, a gender difference in antioxidant metabolism has previously been described in some pathologies, with females being more vulnerable to oxidative damage than males.<sup>70-72</sup> It is thus possible that a same autophagy defect results in a more pronounced phenotype in females, antioxidant metabolism acting as a compensatory mechanism in males.

In conclusion, our results show for the first time that autophagy deficiency in OB decreases their mineralizing capacity and triggers an imbalance between OB and OC resulting in a low bone mass phenotype. Autophagy decline, which is generally associated with age,<sup>73,74</sup> could thus be involved in bone aging by favoring generation of reactive oxygen species, OB apoptosis and OC formation and by decreasing the mineralizing capacity of OB.

## Materials and methods

### Cell culture

The rat UMR-106 osteosarcoma cell line<sup>75</sup> was maintained in Dulbecco's modified Eagle medium (Lonza, BE12-604) supplemented with 10% Hyclone fetal calf serum (Thermo Scientific SH30071.03). The UMR-106 GFP-LC3 clone 4 cells correspond to the UMR-106 cell line stably transfected with the pGFP-LC3 construct. These cells are maintained in the same medium in the presence of G418 (800 g/ml, Sigma-Aldrich, G8168). For mineralization, the cells were cultured in  $\alpha$ -MEM (Lonza, BE02-002) supplemented with 10% Hyclone fetal calf serum,  $\text{CaCl}_2$  (1.4 mM; Merck 2382), ascorbic acid (50 g/mL; Sigma-Aldrich A4034) and dexamethasone (20  $\mu$ g/mL; Sigma-Aldrich D8893) for 3 days, and then for 3 additional days in the same medium in the presence of  $\beta$ -glycerophosphate (50 mg/mL; Sigma-Aldrich G9891). ON-TARGET plus SMARTpool siRNA (D, Abgene Ltd for rat *Atg7* (L095596-01) and *Beclin-1* (L-099237-01) were transfected in the UMR-106 cell line using nucleofection and Amaxa solution V (Lonza VCA-1003).

Explant culture from mouse calvariae was performed by cutting calvarial bone in  $2 \times 2 \text{ mm}^2$  pieces and incubating them for 7 days in  $\alpha$ -MEM supplemented with 10% fetal calf serum. The cultures were then maintained for 15 additional days in differentiation media containing  $\text{CaCl}_2$  (1.4 mM), ascorbic acid (50 g/mL) and  $\beta$ -glycerophosphate (50 mg/mL).

### Mineralization analysis

Mineralization was analyzed after culture in mineralizing conditions during 6 and 11 days for UMR-106 and primary osteoblasts, respectively. After fixation in 100% ethanol on ice for 1

hour, the cells were stained with 1% Alizarin red S dye (Alfa Aesar 42746) (pH 4.1). After incubation at room temperature for 10 minutes, wells were washed five times with deionized water and representative photographs were taken. Mineralized nodules were counted using an optical microscope (10 wells/condition).

### **TRAP staining and RANKL ELISA**

TRAP staining was performed using a leukocyte acid phosphatase kit (Sigma-Aldrich 387A). After 7-9 days of culture in mineralization conditions, conditioned medium was collected from bone explant cultures and RANKL levels were determined by ELISA according to manufacturer's instructions (R&D Systems MTR00).

### **Mice**

*Atg5<sup>flox/flox</sup> Coll-Cre<sup>+</sup>* mice were generated by intercrossing the progeny of crosses between *Atg5<sup>flox/flox</sup>* mice<sup>25</sup> obtained from the RIKEN BioResource Center, Japan (Ref RBRC 02975), and  *$\alpha 1(I)collagen-Cre$*  transgenic mice<sup>26</sup> obtained from the MMRRC (Mice ID number 208-UCD).

### **Genomic DNA isolation and PCR**

Genomic DNA preparation from cortical bone was previously described (34). Briefly, after removing the epiphysis of femurs and tibias and flushing the bone marrow with PBS, the bone surface was scraped with a scalpel. Bone pieces were then digested with collagenase (1 mg/ml type I:II, ratio 1:3, Life Technologies SAS 17100-017 and 17101-015) in Hank's balanced salt solution (Life Technologies SAS 14025-050) containing 0.1 % bovine serum albumin and 1

mM CaCl<sub>2</sub>. Six consecutive 15 minute digestions at 37°C were performed to remove the cells on the bone surface. After washing in PBS, bone pieces were decalcified in 14% EDTA for 1 week and *digested* with proteinase K (0.5 mg/ml in 10mM Tris, pH 8.0, 100mM NaCl, 20mM EDTA, and 1% SDS) at 55 °C overnight. Genomic DNA was then isolated by phenol/chloroform extraction and ethanol precipitation. Bone DNA extracted from *Atg5<sup>flox-flox</sup>* Col1A-Cre<sup>-</sup> or *Atg5<sup>flox-flox</sup>* Col1A-Cre<sup>+</sup> were analyzed by PCR, performed by using Platinum Taq polymerase (Life technologies 10966-034) and primers previously described to amplify *Atg5 flox* or *Atg5* deleted allele<sup>25</sup>. Amplification conditions were 94°C, 3 min (94°C, 30 sec ; 60°C, 30 sec ; 72°C, 1 min) cycled 30 times, 72°C 5 min.

### **RNA isolation and real-time PCR**

Frozen calvaria were pulverized in a Bessler mortar and pestle cooled with dry ice, and total RNAs were extracted from the bone powder using Trizol reagent (Life technologies 15596-018) according to the manufacturer's instruction. Total RNAs (1 µg) were then reverse-transcribed using SuperScript<sup>TM</sup> II Reverse Transcriptase (Life technologies 18064-014) and random hexamer primer (Life technologies N8080127). Triplicates of each 10 fold diluted cDNAs were subjected to real-time PCR analysis in an ABI PRISM 7000 system (Applied Biosystems, Life Technologies SAS, Villebon sur Yvette, France). Reactions were performed in a 20 µl final volume using 5 µl of diluted cDNAs and MESA GREEN qPCR Mastermix Plus (Eurogentec RT-SY2X-03+WOU LR). Amplification conditions were : 95°C, 2 min (95°C, 15 sec ; 60°C, 1 min) cycled 40 times. Nucleotide sequences of PCR primers were as follows :

*Coll1a1* (alpha-1 type 1 collagen) : 5'-GCCAAGGCAACAGTCGCT-3' (forward) and 5'-CTTGGTGGTTTTGTATTCGATGAC-3' (reverse) ; *Runx2* (runt related transcription factor 2) : 5'-TTTAGGGCGCATTCCTCATC-3' (forward) and 5'-TGTCCTTGTGGATTAAGGACTTG-3' (reverse) ; *OPN* (*SPP1*, osteopontin) : 5'-CTGTGTCCTCTGAAGAAAAGGATG-3' (forward) and 5'-GCTTTCATTGGAATTGCTTGG-3' (reverse) ; *36B4* (*Rplp0*, ribosomal protein large P0) : 5'-Tccaggctttgggcatca-3' (forward) and 5'-ctttatcagctgcacatcactcaga-3' (reverse).

Cycle threshold (Ct) were obtained graphically (ABI PRISM 7000 Sequence Detection System version 1.2.3). Gene expression was normalized to *36B4* and  $\Delta$ Ct values calculated.

Comparison of gene expression between two samples (*Atg5<sup>flox-flox</sup>* Col1A-Cre- and *Atg5<sup>flox-flox</sup>* Col1A-Cre+ bone RNAs) was obtained by subtraction of  $\Delta$ Ct values between the two samples to give  $\Delta\Delta$ Ct value. Relative expression was calculated as  $2^{-\Delta\Delta Ct}$  normalized to the *Atg5<sup>flox-flox</sup>* Col1A-Cre- sample.

### **Protein extraction and Western blot analysis**

Cells were washed with phosphate-buffered saline (PBS), scraped in ice-cold PBS and centrifuged at 500 g for 5 min. The cell pellets were resuspended directly in reducing sample buffer (Laemmli : 60 mM Tris-HCl, pH 6.8, 2% sodium dodecyl sulphate (SDS), 100 mM dithiothreitol and 0.01% Bromophenol Blue) in the presence of a complete EDTA-free protease inhibitors cocktail (Roche Diagnostics 04693159001). Genomic DNA was sheared by passage through a narrow-gauge syringe in order to reduce viscosity and resulting total protein extracts were then heated at 95°C for 4 min. [Regarding protein extraction from cortical bone, after removing the epiphysis of femurs and tibias and flushing the bone marrow](#)

with PBS, the bone surface was scraped with a scalpel. Bone pieces were then pulverize in liquid nitrogen and demineralized in EDTA. The resulting bone powder was then incubated in reducing sample buffer containing 2% SDS, 0.5% Sodium deoxycholate, 1% Igepal CA-630 (Nonidet P-40) and 0,1 M dithiothreitol for 10 min at 100°C.

Proteins were separated on a SDS-polyacrylamide gel and electrotransferred to polyvinylidene difluoride membranes (Immobilon, Millipore, Dutscher 44087). Blots were blocked for 1 h with Tris-buffered saline-0.05% Tween 20 (TBS-T) supplemented with 5% nonfat milk and incubated overnight at 4°C with primary antibody. Filters were then washed in TBS-T, incubated for 45 min at room temperature with appropriate secondary antibodies conjugated to horseradish peroxydase and washed again prior to detection of signal with ECL plus chemilumiscent detection kit (Thermo Scientific 80196). Primary antibodies used in this study were rabbit polyclonal anti-LC3 (L8918), rabbit polyclonal anti-ATG7 (A2856), mouse monoclonal anti- $\beta$ -actin (clone AC-15, A1978) and mouse monoclonal anti- $\alpha$ -tubulin (clone TUB 2.1, T4026) antibodies from Sigma-Aldrich and rabbit polyclonal anti-beclin-1 antibodies from MBL International Corporation (CliniSciences PD017).

### **Transmission electron microscopy**

UMR-106 or calvariae cells were fixed in 1.6% glutaraldehyde (Sigma Aldrich G5882) in 0.1M phosphate immediately after medium removal or centrifugation, respectively. Samples were rinsed with the same buffer and then post-fixed in osmium tetroxide (1%) for 1 h. After rinsing with distilled water, they were then dehydrated through an increasing ethanol series and embedded in epoxy resin. Ultrathin sections (70 nm) were collected on Formvar coated copper grids, stained with uranyl acetate and lead citrate and examined with a Jeol JEM 1400 transmission electron microscope.

## **High-resolution transmission electron microscopy / X-ray microanalysis / Electron diffraction**

For High Resolution Transmission Electron Microscopy (HRTEM), ultrathin sections (70 nm) were cut on a Reichert Ultracut E Microtome (Reichert-Jung, Vienna, Austria). Sections were deposited on copper grids (200 mesh) coated with Formvar and holy carbon film. Samples were analyzed on an HRTEM microscope (JEOL 2100F, Japan) with an acceleration voltage of 200 kV, combining Area Electron Diffraction (SAED) and X-ray spectroscopy (EDX). HRTEM and SAED images were digitally recorded with a Gatan Ultrascan 1000 camera, with acquisition software Gatan Digital Micrograph. The analysis system was EDS-SDD Oxford X-Max. For SAED measurements, the diameter of the selected area was about 1  $\mu\text{m}$  and the camera length was 40 cm. SAED patterns were processed with Process Diffraction v4.3.8.B software.<sup>76</sup>

## **Fluorescence Confocal Microscopy**

GFP-LC3 expressing cells were fixed with PBS containing 1% formaldehyde for 20 min at room temperature, and coverslips were mounted in Mowiol mounting medium. Slides were examined by confocal microscopy using the Zeiss 510 Meta laser scanning microscope and 2011 Zen software. For oxidative stress analysis, the cells were stained with 3  $\mu\text{M}$  CellROX orange reagent (Molecular probes, Life technologies C10443) and Hoechst 33342 by adding the probe to the complete medium and incubating the cells at 37°C for 30 min. The cells were washed in PBS and analyzed by fluorescence microscopy. For confocal live cell imaging, cells were grown in glass bottom 24-wells (PAA 21315231X) and stained with 2.5  $\mu\text{g/mL}$  CellMask orange reagent (Molecular probes, Life technologies C10045) by adding the probe to the complete medium and incubating the cells at 37°C for 5 min. The cells were washed in

PBS and imaged using a Zeiss high-throughput epi-fluorescent microscope, equipped with an EMCCD video camera (Cascade II : 1024), heated incubation chamber with CO<sub>2</sub> and Axiovision image acquisition software (release 4.8.2).

### **Histomorphometric analysis**

Femurs were fixed in 10% neutral buffered formaldehyde. The excised distal femurs were cut longitudinally to expose the bone marrow with a low-speed metallurgical saw and dehydrated in grade ethanol, defatted in toluene, and embedded in methylmethacrylate without decalcification. Five-micrometer-thick longitudinal sections were cut with a Reicher-Jung Polycut microtome and stained with 1% toluidine blue. Histomorphometric analysis was performed on the region between 0.2 and 1.2 mm distal to the growth plate using OsteoMeasure (OsteoMetrics, Atlanta, GA, USA) at a magnification of X200. The variables of cancellous bone volume (BV/TV), trabecular width (Tb.Wi), trabecular number (Tb.N), trabecular separation (Tb.Sp), OB perimeter (OB.Pm) and OC perimeter (OC.Pm) were calculated according to standard formulas and nomenclature established by the American Society for Bone and Mineral Research.<sup>77</sup>

### **Micro-CT analysis**

Architectural parameters were analyzed by high-resolution X-ray micro-CT, using the SkyScan-1076 (SkyScan, Aartselaar, Belgium) system for small-animal imaging. Each femur was scanned parallel to its longitudinal axis (60 kV, 148 A). A core of 100 sections, each 11  $\mu$ m thick (7 mm long) was used for trabecular bone morphometry evaluations with SkyScan CtAn software. The following factors were measured: total volume, bone volume (BV) and the BV/tissue volume (TV) ratio. Trabecular BV and cortical BV were evaluated separately

and the ratio of these two volumes was calculated. Trabecular bone thickness, trabecular number and separation were measured with a semi-automating morphing procedure, from total BV. Cortical thickness was evaluated on 150 sections at mid shaft of diaphysis.

### **Statistical analysis**

The results are expressed as mean  $\pm$  SD and comparisons were performed using Student's t test except for percentage comparison for which the Kruskal-Wallis test was used. All statistics were computed with MINITAB<sup>TM</sup> Inc. V12.2 (State College, PA, USA).

## **Acknowledgments**

The authors would like to gratefully to thank Pascal Staccini (Département Informatique et Information Médicale, CHU de Nice, France) for statistical analysis of the results as well as Xavier Jaurand who performed the high resolution electron microscopic / X-rays microanalysis / electron diffraction study at the Centre Technologique des Microstructures (CT $\mu$ , Lyon, France). The CECIL (CEntre Commun d'Imagerie Laennec, Lyon, France) is also gratefully acknowledged. This work was supported by the CNRS, CEA, Société Française de Rhumatologie, and by a generous gift from Servier and Amgen without conflict of interest.

**Abbreviations list**

BV, bone volume; Col1A, type 1a collagen; OB, osteoblast; OC, osteoclast; OPN, osteopontin; RANKL, receptor activator of NF- $\kappa$ B; Runx2, runt-related transcription factor 2; TRAP, tartrate-resistant alkaline phosphatase; TV, total volume.

## References

1. Raggatt LJ, Partridge NC. Cellular and molecular mechanisms of bone remodeling. *J Biol Chem* 2010; 285:25103-8.
2. Kular J, Tickner J, Chim SM, Xu J. An overview of the regulation of bone remodelling at the cellular level. *Clin Biochem* 2012; 45:863-73.
3. Manolagas SC. From estrogen-centric to aging and oxidative stress: a revised perspective of the pathogenesis of osteoporosis. *Endocr Rev* 2010; 31:266-300.
4. Levine B, Kroemer G. Autophagy in the pathogenesis of disease. *Cell* 2008; 132:27-42.
5. Mizushima N, Levine B, Cuervo AM, Klionsky DJ. Autophagy fights disease through cellular self-digestion. *Nature* 2008; 451:1069-75.
6. Mizushima N. Autophagy: process and function. *Genes Dev* 2007; 21:2861-73.
7. Galluzzi L, Vicencio JM, Kepp O, Tasdemir E, Maiuri MC, Kroemer G. To die or not to die: that is the autophagic question. *Curr Mol Med* 2008; 8:78-91.
8. Debnath J, Baehrecke EH, Kroemer G. Does autophagy contribute to cell death? *Autophagy* 2005; 1:66-74.
9. Hoyer-Hansen M, Bastholm L, Szyniarowski P, Campanella M, Szabadkai G, Farkas T, et al. Control of macroautophagy by calcium, calmodulin-dependent kinase kinase-beta, and Bcl-2. *Mol Cell* 2007; 25:193-205.
10. Hoyer-Hansen M, Nordbrandt SP, Jaattela M. Autophagy as a basis for the health-promoting effects of vitamin D. *Trends Mol Med* 2010; 16:295-302.
11. Pearson KJ, Baur JA, Lewis KN, Peshkin L, Price NL, Labinskyy N, et al. Resveratrol delays age-related deterioration and mimics transcriptional aspects of dietary restriction without extending life span. *Cell Metab* 2008; 8:157-68.
12. Manjithaya R, Subramani S. Autophagy: a broad role in unconventional protein secretion? *Trends Cell Biol* 2011; 21:67-73.
13. Deretic V, Jiang S, Dupont N. Autophagy intersections with conventional and unconventional secretion in tissue development, remodeling and inflammation. *Trends Cell Biol* 2012; 22:397-406.
14. Pan F, Liu XG, Guo YF, Chen Y, Dong SS, Qiu C, et al. The regulation-of-autophagy pathway may influence Chinese stature variation: evidence from elder adults. *J Hum Genet* 2010; 55:441-7.
15. Zhang L, Guo YF, Liu YZ, Liu YJ, Xiong DH, Liu XG, et al. Pathway-based genome-wide association analysis identified the importance of regulation-of-autophagy pathway for ultradistal radius BMD. *J Bone Miner Res* 2010; 25:1572-80.
16. Klionsky DJ, Cuervo AM, Seglen PO. Methods for monitoring autophagy from yeast to human. *Autophagy* 2007; 3:181-206.
17. Klionsky DJ, Agostinis P, Agrawal DK, Aliev G, Askew DS, Baba M, et al. Guidelines for the use and interpretation of assays for monitoring autophagy in higher eukaryotes. *Autophagy* 2008; 4:151-75.
18. Klionsky DJ, Abdalla FC, Abeliovich H, Abraham RT, Acevedo-Arozena A, Adeli K, et al. Guidelines for the use and interpretation of assays for monitoring autophagy. *Autophagy* 2012; 8:445-544.
19. Sarkar S, Davies JE, Huang Z, Tunnacliffe A, Rubinsztein DC. Trehalose, a novel mTOR-independent autophagy enhancer, accelerates the clearance of mutant huntingtin and alpha-synuclein. *J Biol Chem* 2007; 282:5641-52.
20. Mizushima N. Methods for monitoring autophagy. *Int J Biochem Cell Biol* 2004; 36:2491-502.
21. Ichimura Y, Kirisako T, Takao T, Satomi Y, Shimonishi Y, Ishihara N, et al. A ubiquitin-like system mediates protein lipidation. *Nature* 2000; 408:488-92.

22. Itakura E, Kishi C, Inoue K, Mizushima N. Beclin 1 forms two distinct phosphatidylinositol 3-kinase complexes with mammalian Atg14 and UVRAG. *Mol Biol Cell* 2008; 19:5360-72.
23. Matsunaga K, Saitoh T, Tabata K, Omori H, Satoh T, Kurotori N, et al. Two Beclin 1-binding proteins, Atg14L and Rubicon, reciprocally regulate autophagy at different stages. *Nat Cell Biol* 2009; 11:385-96.
24. Zhong Y, Wang QJ, Li X, Yan Y, Backer JM, Chait BT, et al. Distinct regulation of autophagic activity by Atg14L and Rubicon associated with Beclin 1-phosphatidylinositol-3-kinase complex. *Nat Cell Biol* 2009; 11:468-76.
25. Hara T, Nakamura K, Matsui M, Yamamoto A, Nakahara Y, Suzuki-Migishima R, et al. Suppression of basal autophagy in neural cells causes neurodegenerative disease in mice. *Nature* 2006; 441:885-9.
26. Dacquin R, Starbuck M, Schinke T, Karsenty G. Mouse alpha1(I)-collagen promoter is the best known promoter to drive efficient Cre recombinase expression in osteoblast. *Dev Dyn* 2002; 224:245-51.
27. Rana T, Schultz MA, Freeman ML, Biswas S. Loss of Nrf2 accelerates ionizing radiation-induced bone loss by upregulating RANKL. *Free Radic Biol Med* 2012; 53:2298-307.
28. Choi EM. Protective effect of quercitrin against hydrogen peroxide-induced dysfunction in osteoblastic MC3T3-E1 cells. *Exp Toxicol Pathol* 2012; 64:211-6.
29. Baek KH, Oh KW, Lee WY, Lee SS, Kim MK, Kwon HS, et al. Association of oxidative stress with postmenopausal osteoporosis and the effects of hydrogen peroxide on osteoclast formation in human bone marrow cell cultures. *Calcif Tissue Int* 2010; 87:226-35.
30. Hocking LJ, Whitehouse C, Helfrich MH. Autophagy: a new player in skeletal maintenance? *J Bone Miner Res* 2012; 27:1439-47.
31. Jia J, Yao W, Guan M, Dai W, Shahnazari M, Kar R, et al. Glucocorticoid dose determines osteocyte cell fate. *FASEB J* 2011; 25:3366-76.
32. Zahm AM, Bohensky J, Adams CS, Shapiro IM, Srinivas V. Bone cell autophagy is regulated by environmental factors. *Cells Tissues Organs* 2011; 194:274-8.
33. Xia X, Kar R, Gluhak-Heinrich J, Yao W, Lane NE, Bonewald LF, et al. Glucocorticoid-induced autophagy in osteocytes. *J Bone Miner Res* 2010; 25:2479-88.
34. Onal M, Piemontese M, Xiong J, Wang Y, Han L, Ye S, et al. Suppression of Autophagy in Osteocytes Mimics Skeletal Aging. *J Biol Chem* 2013.
35. Whitehouse CA, Waters S, Marchbank K, Horner A, McGowan NW, Jovanovic JV, et al. Neighbor of Brca1 gene (Nbr1) functions as a negative regulator of postnatal osteoblastic bone formation and p38 MAPK activity. *Proc Natl Acad Sci U S A* 2010; 107:12913-8.
36. DeSelm CJ, Miller BC, Zou W, Beatty WL, van Meel E, Takahata Y, et al. Autophagy proteins regulate the secretory component of osteoclastic bone resorption. *Dev Cell* 2011; 21:966-74.
37. Pantovic A, Krstic A, Janjetovic K, Kocic J, Harhaji-Trajkovic L, Bugarski D, et al. Coordinated time-dependent modulation of AMPK/Akt/mTOR signaling and autophagy controls osteogenic differentiation of human mesenchymal stem cells. *Bone* 2013; 52:524-31.
38. Huitema LF, Vaandrager AB. What triggers cell-mediated mineralization? *Front Biosci* 2007; 12:2631-45.
39. Hoshi K, Ozawa H. Matrix vesicle calcification in bones of adult rats. *Calcif Tissue Int* 2000; 66:430-4.
40. Anderson HC. Matrix vesicles and calcification. *Curr Rheumatol Rep* 2003; 5:222-6.
41. Rohde M, Mayer H. Exocytotic process as a novel model for mineralization by osteoblasts in vitro and in vivo determined by electron microscopic analysis. *Calcif Tissue Int* 2007; 80:323-36.
42. Mahamid J, Sharir A, Gur D, Zelzer E, Addadi L, Weiner S. Bone mineralization proceeds

- through intracellular calcium phosphate loaded vesicles: a cryo-electron microscopy study. *J Struct Biol* 2011; 174:527-35.
43. Stanford CM, Jacobson PA, Eanes ED, Lembke LA, Midura RJ. Rapidly forming apatitic mineral in an osteoblastic cell line (UMR 106-01 BSP). *J Biol Chem* 1995; 270:9420-8.
  44. Boonrungsiman S, Gentleman E, Carzaniga R, Evans ND, McComb DW, Porter AE, Stevens MM. The role of intracellular calcium phosphate in osteoblast-mediated bone apatite formation. *Proc Natl Acad Sci U S A*. 2012;109:14170-5.
  45. Azari F, Vali H, Guerquin-Kern JL, Wu TD, Croisy A, Sears SK, et al. Intracellular precipitation of hydroxyapatite mineral and implications for pathologic calcification. *J Struct Biol* 2008; 162:468-79.
  46. Manjithaya R, Anjard C, Loomis WF, Subramani S. Unconventional secretion of *Pichia pastoris* Acb1 is dependent on GRASP protein, peroxisomal functions, and autophagosome formation. *J Cell Biol* 2010; 188:537-46.
  47. Duran JM, Anjard C, Stefan C, Loomis WF, Malhotra V. Unconventional secretion of Acb1 is mediated by autophagosomes. *J Cell Biol* 2010; 188:527-36.
  48. Dupont N, Jiang S, Pilli M, Ornatowski W, Bhattacharya D, Deretic V. Autophagy-based unconventional secretory pathway for extracellular delivery of IL-1beta. *EMBO J* 2011; 30:4701-11.
  49. Bruns C, McCaffery JM, Curwin AJ, Duran JM, Malhotra V. Biogenesis of a novel compartment for autophagosome-mediated unconventional protein secretion. *J Cell Biol* 2011; 195:979-92.
  50. Fader CM, Aguilera MO, Colombo MI. ATP is released from autophagic vesicles to the extracellular space in a VAMP7-dependent manner. *Autophagy* 2012; 8:1741-56.
  51. Sirois I, Groleau J, Pallet N, Brassard N, Hamelin K, Londono I, et al. Caspase activation regulates the extracellular export of autophagic vacuoles. *Autophagy* 2012; 8:927-37.
  52. Griffiths RE, Kupzig S, Cogan N, Mankelov TJ, Betin VM, Trakarnsanga K, et al. Maturing reticulocytes internalize plasma membrane in glycophorin A-containing vesicles that fuse with autophagosomes before exocytosis. *Blood* 2012; 119:6296-306.
  53. Kim DH, Davis RC, Furukawa R, Fechheimer M. Autophagy contributes to degradation of Hirano bodies. *Autophagy* 2009; 5:44-51.
  54. Lee J, Giordano S, Zhang J. Autophagy, mitochondria and oxidative stress: cross-talk and redox signalling. *Biochem J* 2012; 441:523-40.
  55. Jagger CJ, Lean JM, Davies JT, Chambers TJ. Tumor necrosis factor-alpha mediates osteopenia caused by depletion of antioxidants. *Endocrinology* 2005; 146:113-8.
  56. Almeida M, Han L, Ambrogini E, Bartell SM, Manolagas SC. Oxidative stress stimulates apoptosis and activates NF-kappaB in osteoblastic cells via a PKCbeta/p66shc signaling cascade: counter regulation by estrogens or androgens. *Mol Endocrinol* 2010; 24:2030-7.
  57. Almeida M, Han L, Martin-Millan M, Plotkin LI, Stewart SA, Roberson PK, et al. Skeletal involution by age-associated oxidative stress and its acceleration by loss of sex steroids. *J Biol Chem* 2007; 282:27285-97.
  58. Karsenty G, Ducy P, Starbuck M, Priemel M, Shen J, Geoffroy V, et al. Cbfa1 as a regulator of osteoblast differentiation and function. *Bone* 1999; 25:107-8.
  59. Ducy P, Starbuck M, Priemel M, Shen J, Pinero G, Geoffroy V, et al. A Cbfa1-dependent genetic pathway controls bone formation beyond embryonic development. *Genes Dev* 1999; 13:1025-36.
  60. Bellido T, Ali AA, Plotkin LI, Fu Q, Gubrij I, Roberson PK, et al. Proteasomal degradation of Runx2 shortens parathyroid hormone-induced anti-apoptotic signaling in osteoblasts. A putative explanation for why intermittent administration is needed for bone anabolism. *J Biol Chem* 2003; 278:50259-72.
  61. Ho WP, Chan WP, Hsieh MS, Chen RM. Runx2-mediated bcl-2 gene expression

- contributes to nitric oxide protection against hydrogen peroxide-induced osteoblast apoptosis. *J Cell Biochem* 2009; 108:1084-93.
62. Browne G, Nesbitt H, Ming L, Stein GS, Lian JB, McKeown SR, et al. Bicalutamide-induced hypoxia potentiates RUNX2-mediated Bcl-2 expression resulting in apoptosis resistance. *Br J Cancer* 2012; 107:1714-21.
63. Ardura JA, Sanz AB, Ortiz A, Esbrit P. Parathyroid hormone-related protein protects renal tubuloepithelial cells from apoptosis by activating transcription factor Runx2. *Kidney Int* 2013.
64. Wang KX, Denhardt DT. Osteopontin: role in immune regulation and stress responses. *Cytokine Growth Factor Rev* 2008; 19:333-45.
65. Kaushik S, Singh R, Cuervo AM. Autophagic pathways and metabolic stress. *Diabetes Obes Metab* 2010; 12 Suppl 2:4-14.
66. Hamamura K, Yokota H. Stress to endoplasmic reticulum of mouse osteoblasts induces apoptosis and transcriptional activation for bone remodeling. *FEBS Lett* 2007; 581:1769-74.
67. Noh T, Gabet Y, Cogan J, Shi Y, Tank A, Sasaki T, et al. Lef1 haploinsufficient mice display a low turnover and low bone mass phenotype in a gender- and age-specific manner. *PLoS One* 2009;4:e5438.
68. Yao W, Cheng Z, Shahnazari M, Dai W, Johnson ML, Lane NE. Overexpression of secreted frizzled-related protein 1 inhibits bone formation and attenuates parathyroid hormone bone anabolic effects. *J Bone Miner Res* 2010;25:190-9.
69. Pennypacker B, Shea M, Liu Q, Masarachia P, Saftig P, Rodan S, et al. Bone density, strength, and formation in adult cathepsin K (-/-) mice. *Bone* 2009;44:199-207.
70. Schuessel K, Leutner S, Cairns NJ, Müller WE, Eckert A. Impact of gender on upregulation of antioxidant defence mechanisms in Alzheimer's disease brain. *J Neural Transm* 2004;111:1167-82.
71. Kikuchi A, Takeda A, Onodera H, Kimpara T, Hisanaga K, Sato N, et al. Systemic increase of oxidative nucleic acid damage in Parkinson's disease and multiple system atrophy. *Neurobiol Dis* 2002;9:244-8.
72. Vassalle C, Maffei S, Boni C, Zucchelli GC. Gender-related differences in oxidative stress levels among elderly patients with coronary artery disease. *Fertil Steril* 2008;89:608-13.
73. Cuervo AM. Autophagy and aging: keeping that old broom working. *Trends Genet* 2008; 24:604-12.
74. Rubinsztein DC, Marino G, Kroemer G. Autophagy and aging. *Cell* 2011; 146:682-95.
75. Partridge NC, Alcorn D, Michelangeli VP, Ryan G, Martin TJ. Morphological and biochemical characterization of four clonal osteogenic sarcoma cell lines of rat origin. *Cancer Res* 1983; 43:4308-14.
76. Labar JL. Consistent indexing of a (set of) single crystal SAED pattern(s) with the ProcessDiffraction program. *Ultramicroscopy* 2005; 103:237-49.
77. Dempster DW, Compston JE, Drezner MK, Glorieux FH, Kanis JA, Malluche H, et al. Standardized nomenclature, symbols, and units for bone histomorphometry: a 2012 update of the report of the ASBMR Histomorphometry Nomenclature Committee. *J Bone Miner Res* 2013; 28:2-17.

## Figure legends

**Figure 1. Mineralization is associated with an autophagy induction in the UMR-106 osteoblastic cell line.** (A) UMR-106 cells were cultured in mineralization medium and proteins were extracted at day 3, 4 and 5. Western blot of LC3 and  $\beta$ -actin, representative of three experiments. LC3-II to  $\beta$ -actin relative levels are presented. Mean and standard errors are shown. Statistical significance was determined by Student's t-test (\* $p < 0.05$ ). (B) Optical and confocal microscopy analysis of GFP-LC3 expressing UMR-106 cell line at day 3 and 5 during mineralization, representative of three experiments. Black and white arrows indicate mineralization foci (F) and autophagic cells, respectively. (C) Electron microscopy of mineralizing UMR-106 cells. White arrows indicate autophagic vesicles. Black arrows indicate mineralization crystal-like structures. The dashed line delimitates the extracellular medium; mtc, mitochondria. (D) High-resolution transmission electron microscopy of the crystal-like structures. (E) X-ray microanalysis indicating the components of the crystal-like structures. (F) Electron diffraction of the crystal-like structures. Arrows point to the reflections of hydroxyapatite.

**Figure 2. Mineralization is associated with an autophagy induction in mouse primary osteoblasts.** (A) Mouse primary osteoblasts were cultured in mineralization medium and proteins were extracted at day 5 and 12. Western blot of LC3 and  $\beta$ -actin at day 5 and 12 during mineralization in primary mouse OB, representative of three experiments. LC3-II to  $\beta$ -actin relative levels are presented. Mean and standard errors are shown. Statistical significance was determined by Student's t-test (\*\* $p < 0.005$ ). (B) Electron microscopy of mineralizing primary OB. The area included in the black square is enlarged. White arrows indicate autophagic vesicles. Black arrows indicate mineralization crystal-like structures that

can be light or very dense. mtc, mitochondria; N, nucleus. (C) High-resolution transmission electron microscopy of the crystal-like structures. (D) X-ray microanalysis indicating the components of the crystal-like structures. (E) Electron diffraction of the crystal-like structures.

**Figure 3. Knockdown of autophagy genes reduces mineralization capacity in the UMR-106 cell line.** (A) Western blot of Atg7 and  $\alpha$ -tubulin, 24 h after siRNA transfection in UMR-106 cells, representative of three experiments. siC, control siRNA; siATG7, *Atg7* siRNA. (B) Alizarin red staining of mineralization nodules, representative of four experiments. UMR-106 cells were transfected with siRNA and cultured in mineralization medium for 5 days. Upper panels: representative pictures of the wells; lower panels: representative pictures of mineralization foci (dark spots, x 2.5 magnification). (C) Mean number of mineralization nodules in each condition, ten wells per condition, representative of four experiments. (D) Western blot of Beclin-1 and  $\alpha$ -actin, 48 h after siRNA transfection in UMR-106 cells, representative of three experiments. siC, control siRNA; siBECN1, *Beclin-1* siRNA. (E) Alizarin red staining of mineralization nodules, representative of three experiments. UMR-106 cells were transfected with siRNA and cultured in mineralization medium for 5 days. Upper panels: representative pictures of the wells; lower panels: representative pictures of mineralization foci (dark spots, x 2.5 magnification). (F) Mean number of mineralization nodules in each condition, ten wells per condition, representative of three experiments.

**Figure 4. *Atg5* deficiency in osteoblasts results in decreased mineralization.** Alizarine red staining of mineralization in calvaria bone explant cultures from control (*Atg5<sup>flox-flox</sup>* Col1A-

Cre-) and mutant ( $Atg5^{flox-flox}$  Col1A-Cre+) mice, representative of three experiments. B, bone explant.

**Figure 5. *Atg5* deficiency in osteoblasts stimulates OC generation in calvarial explants.**

(A-B) Representative photographs of TRAP staining in calvarial bone explants from control ( $Atg5^{flox-flox}$  Col1A-Cre-) and mutant ( $Atg5^{flox-flox}$  Col1A-Cre+) mice, representative of four experiments. Cultures from mutant mice exhibit 7-fold OC number compared to cultures from control littermates (mean:  $77 \pm 37$  in mutant vs  $10 \pm 8$  in control cultures). Each well represents a single calvaria. B, bone explant. (C) Secreted RANKL measured in the conditioned medium of calvarial bone explants from control and mutant mice. Each dot represents the result obtained for one calvaria (n=5) and the line shows the median. \*p < 0.05 vs respective  $Atg5^{flox-flox}$  Col1A-Cre- by Student's t test. (D) Oxidative stress in bone explant cultures from control and mutant mice, 4 mice per condition. Representative photographs of both conditions and mean fluorescence intensity measured in 240 cells per condition. (E) Relative expression level of Runx2, OPN and COLL mRNA in calvariae from female mutant mice compared with female control mice determined by quantitative RT-PCR. Results are presented as mean  $\pm$  SD (n=4). \*p < 0.05 vs control by Student's t test.

**Figure 6. Bone mass is decreased following *Atg5* deletion. (A-F) Histomorphometric**

analysis of female and male nine-month-old  $Atg5^{flox-flox}$  Col1A-Cre+ mice and their control littermates. Bars indicate mean  $\pm$  SD. C,  $Atg5^{flox-flox}$  Col1A-Cre- mice, females: n=8, males: n=9; M,  $Atg5^{flox-flox}$  Col1A-Cre+ mice, females: n=9, males: n=9. (A) Percentage of bone volume per total volume (BV/TV). (B) Trabecular width (Tb.Wi). (C) Trabecular number per

mm (Tb.N). (D) Trabecular space (Tb.Sp). (E) Percentage of trabecular bone surface covered by osteoblast (OB Pm). (F) Percentage of trabecular bone surface covered by OC (OC Pm). (G) OB to OC ratio (%) in female and male control and mutant mice. \*p < 0.05 vs control by Student's t test.

**Figure 7. 3D reconstruction of distal femur trabecular bone using microCT.** Wild-type and mutant female mice femurs were collected at 9 months of age. These reconstructions based on 100 sections analysis, illustrate the decrease of trabecular bone volume in *Atg5<sup>flox-flox</sup> Col1A-Cre+* mutant mice.

### Online supplemental material

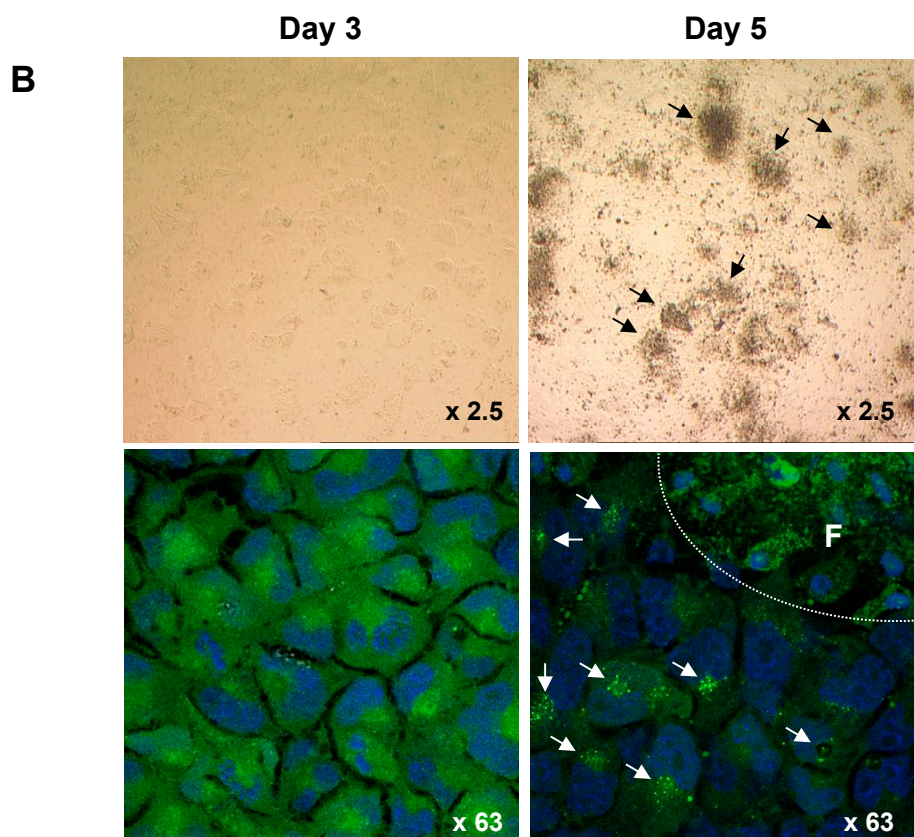
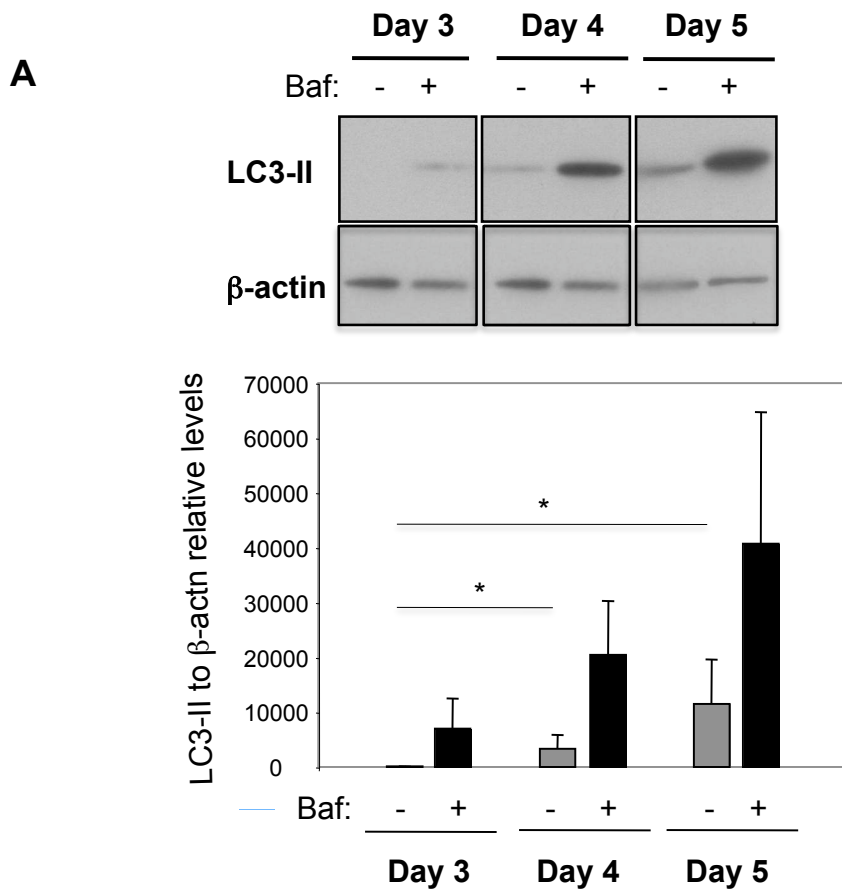
**Movie 1. Autophagosomes movement in mineralizing OB cell line stably expressing a GFP-LC3 construct.** The movie shows autophagosomes (green dots, arrows) moving to the cell membrane stained with CellMask orange reagent, in mineralizing GFP-LC3 expressing UMR-106 cells. The cells were analyzed by confocal time-lapse video using a Zeiss high-throughput epi-fluorescent microscope and frames were taken every minute for 15 minutes.

**Supplementary Figure S1. Atg5 gene deletion in bones of *Atg5<sup>flox-flox</sup> Col1A-Cre+* mice.**

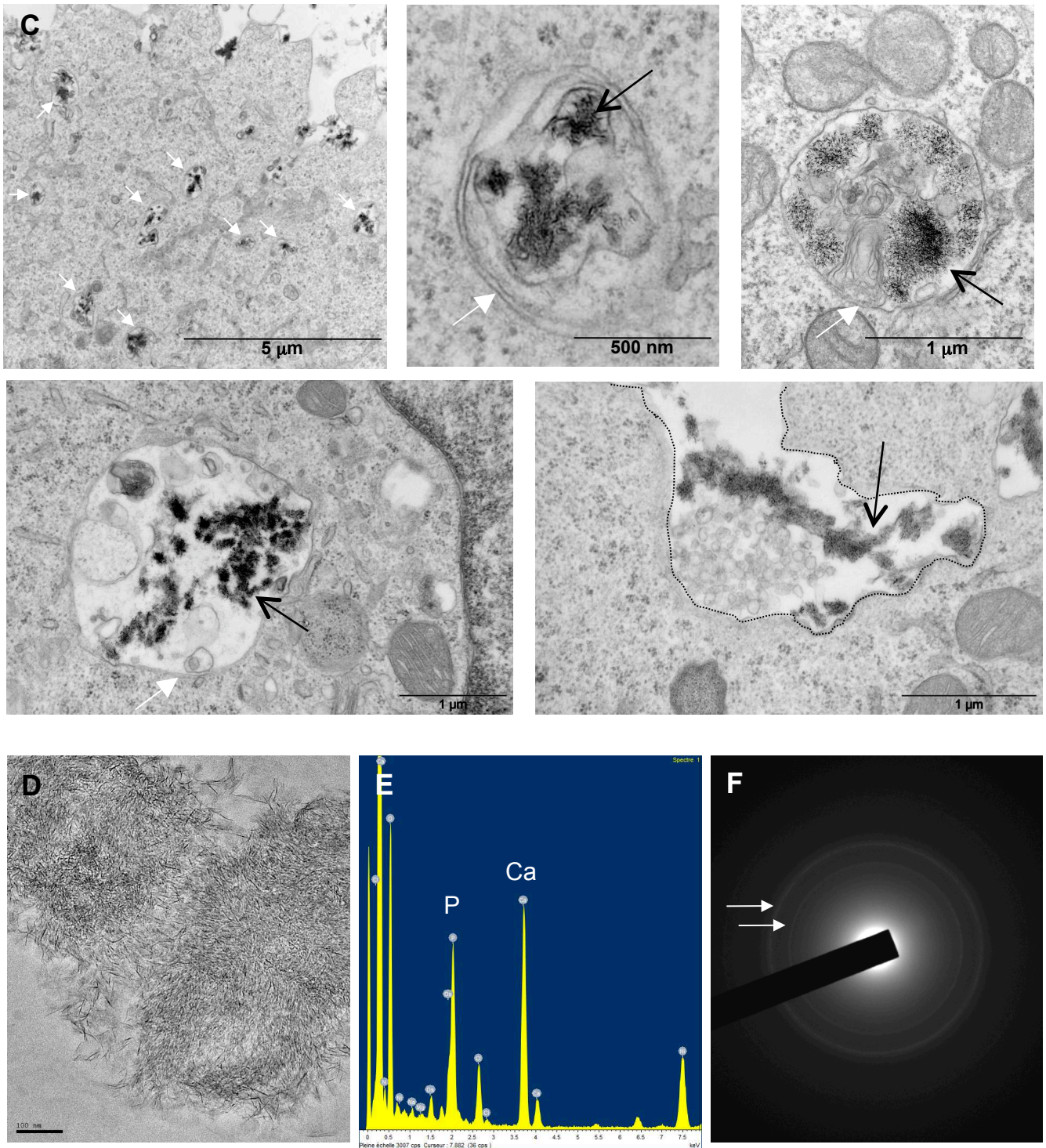
(A) Position of the PCR primers in the flox allele and the deleted allele (from Hara *et al.*, 2006 (25)). Primers P1 and P2 are used for amplification of the *flox* allele and primers P2 and P3 for the deleted allele. (B) Genomic DNA extracted from cortical bone of three *Atg5<sup>flox-flox</sup>*

*flox* Col1A-Cre- and three *Atg5<sup>flox-flox</sup>* Col1A-Cre+ mice was analyzed by PCR using primers P1, P2 and P3. (C) Western blot analysis of LC3 in cortical bone of control and mutant mice and quantification.  $\beta$ -actin was used as a loading control.

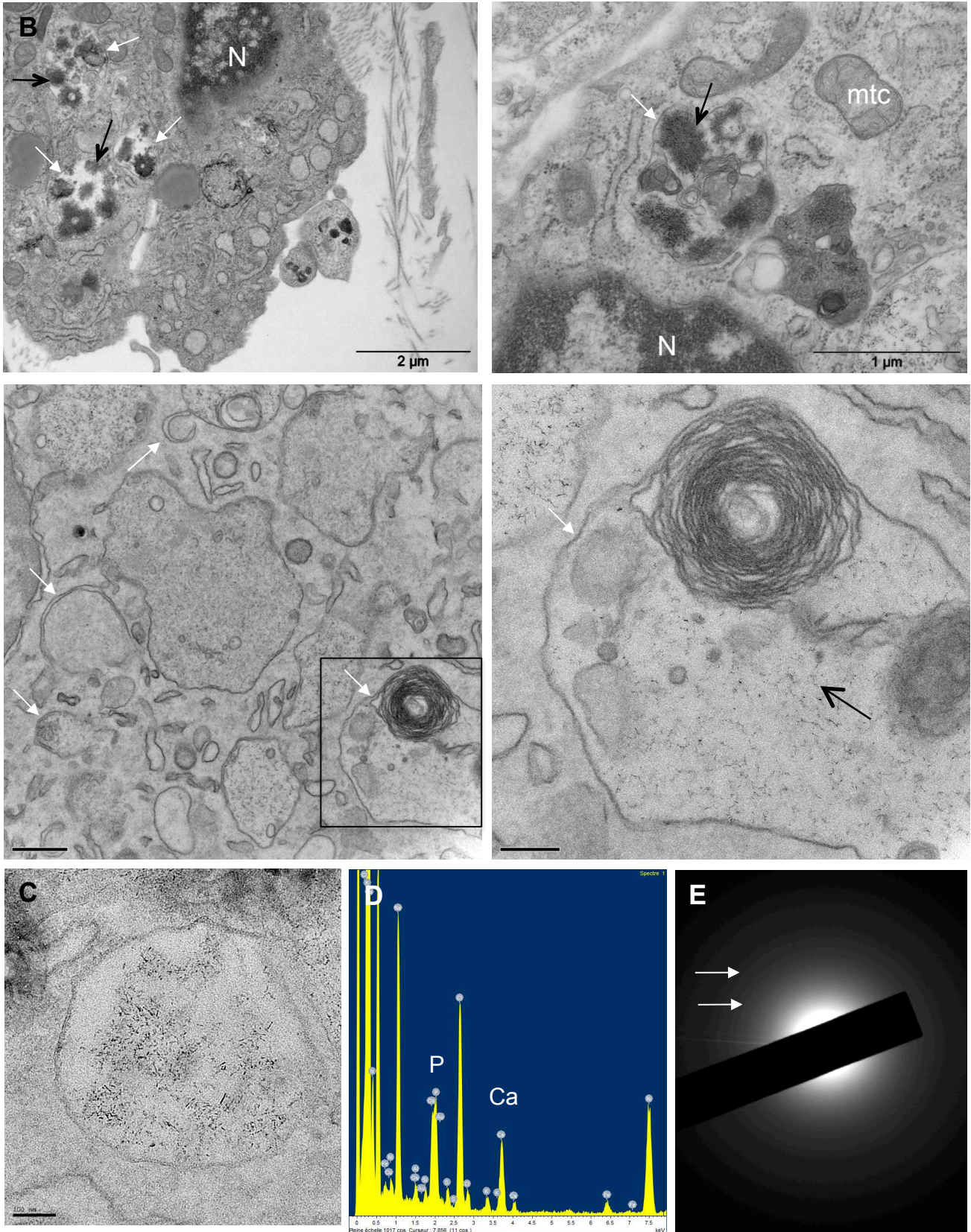
**Supplementary Figure S2. Bone histology of *Atg5<sup>flox-flox</sup>* Col1A-Cre- and *Atg5<sup>flox-flox</sup>* Col1A-Cre+ mice.** (A) Histology of femur from control and mutant 9 month-old mice after toluidine blue staining (x 40 magnification). (B) Osteoblasts (white arrows) identified in femur sections (x 200 magnification). (C) Osteoclasts (white arrows) identified in femur sections (x 200 magnification).



Nollet et al. Figure 1 A-B

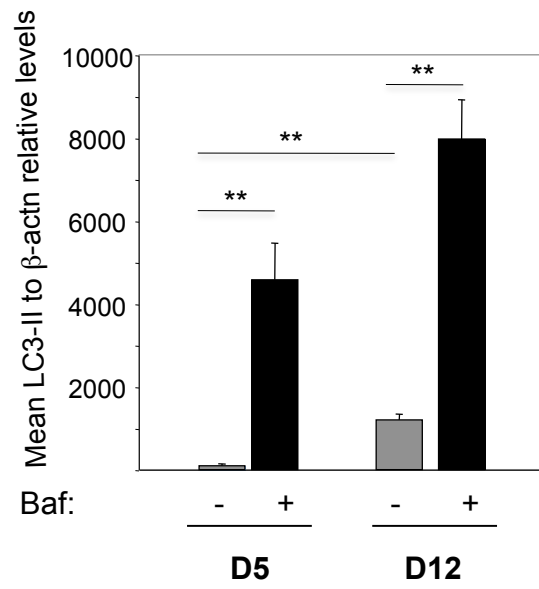
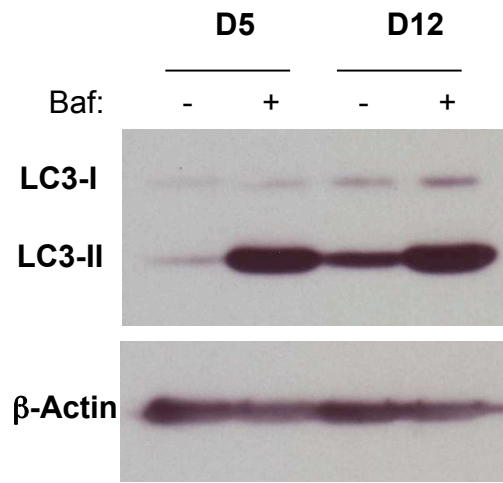


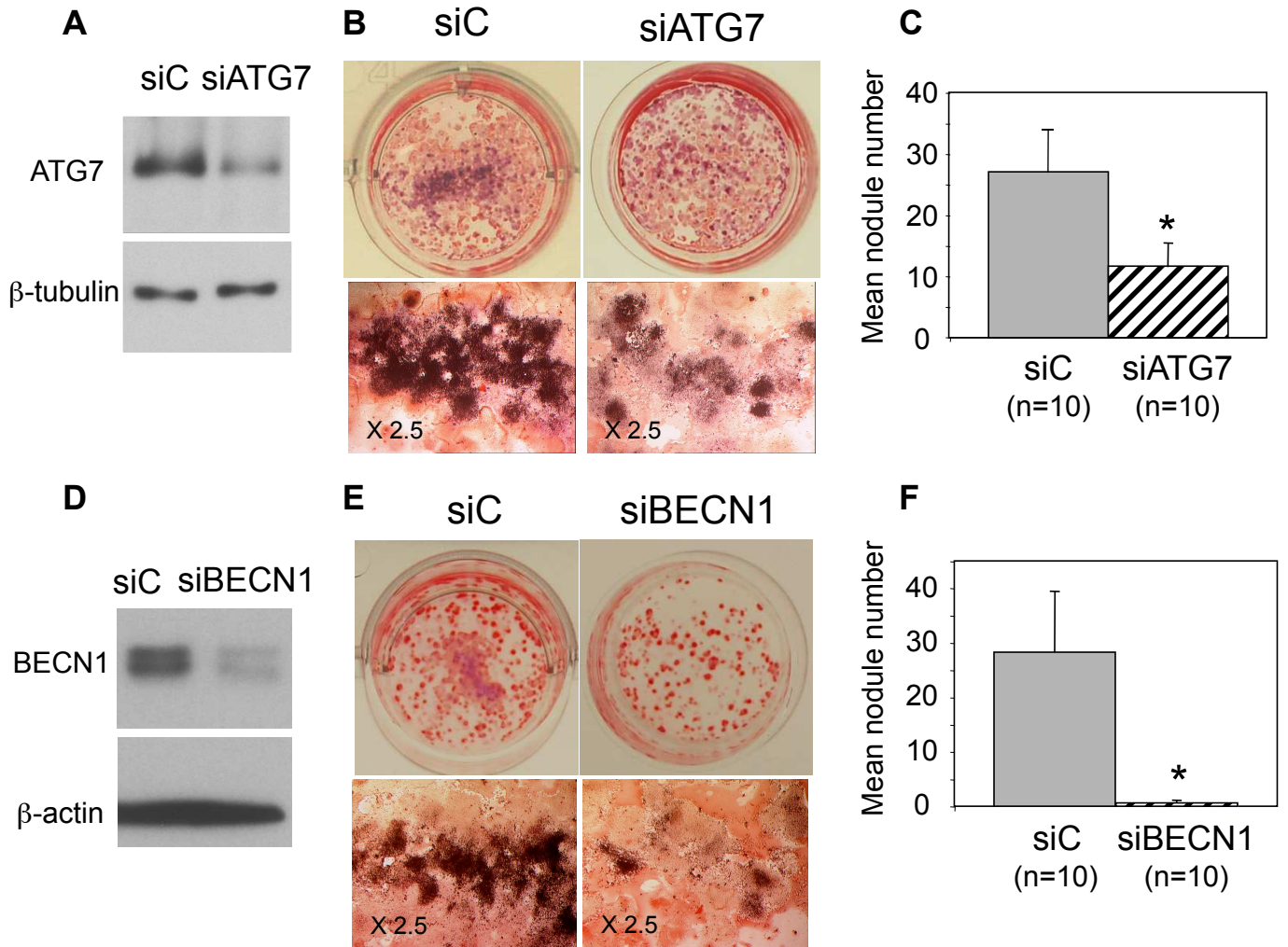
Nollet et al. Figure 1 C-F

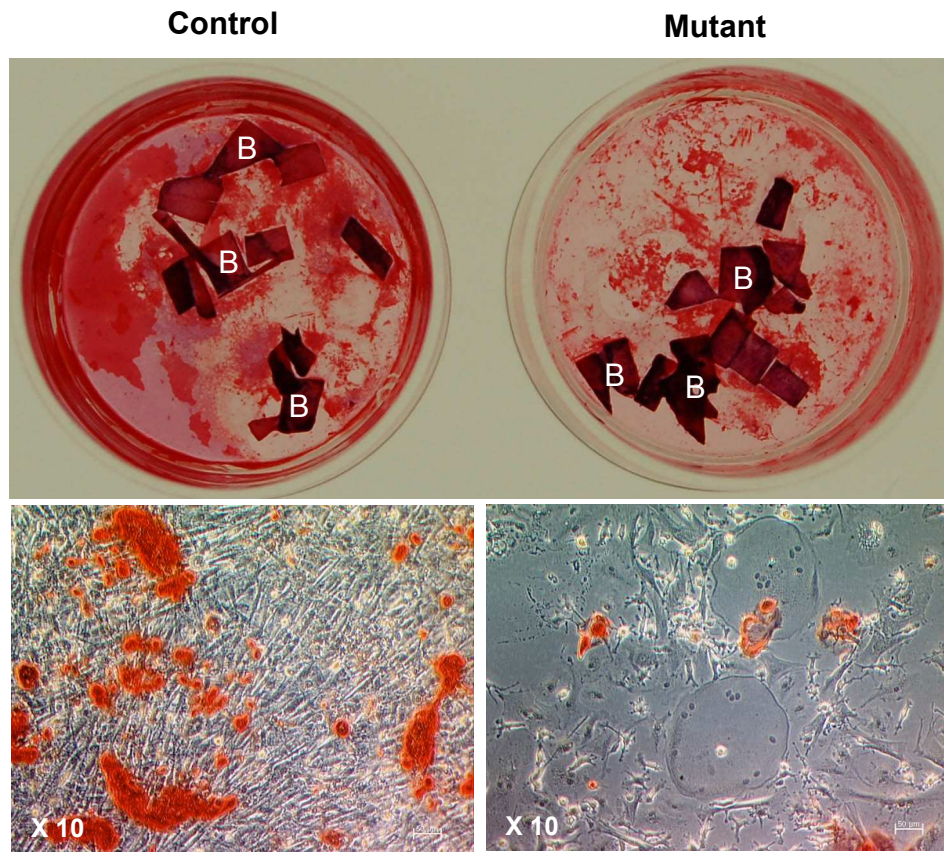


Nollet et al. Figure 2 B-E

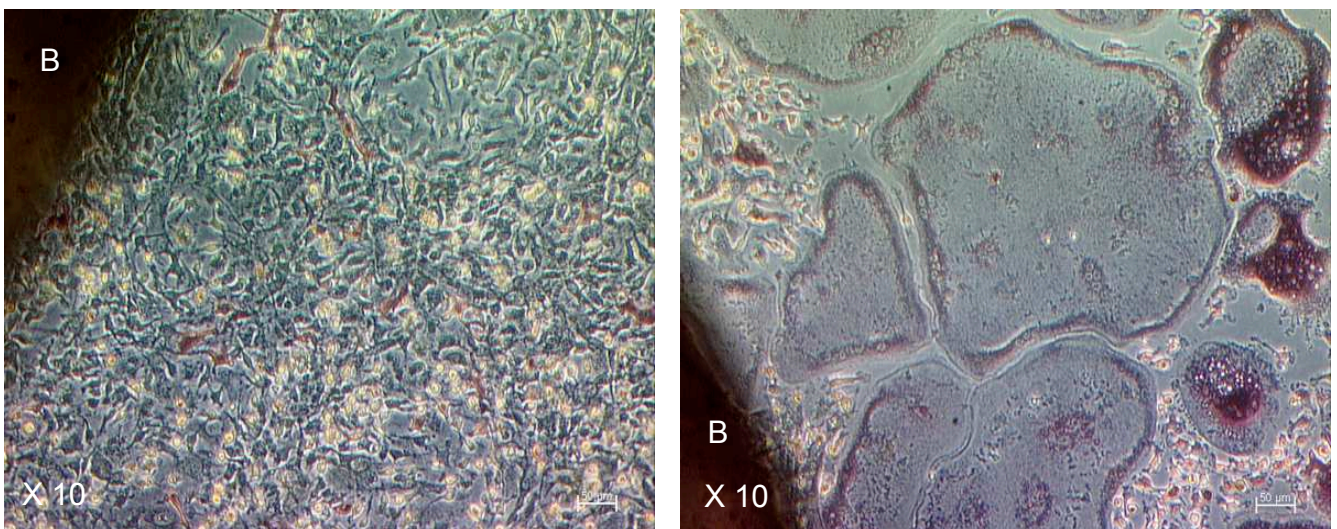
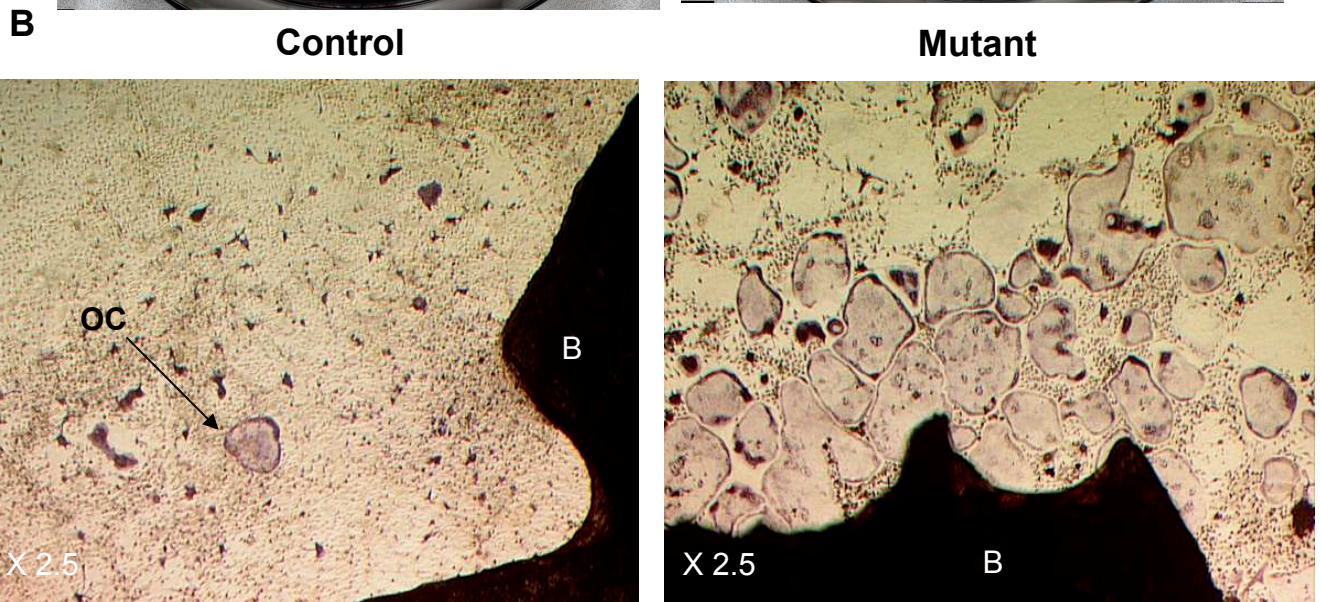
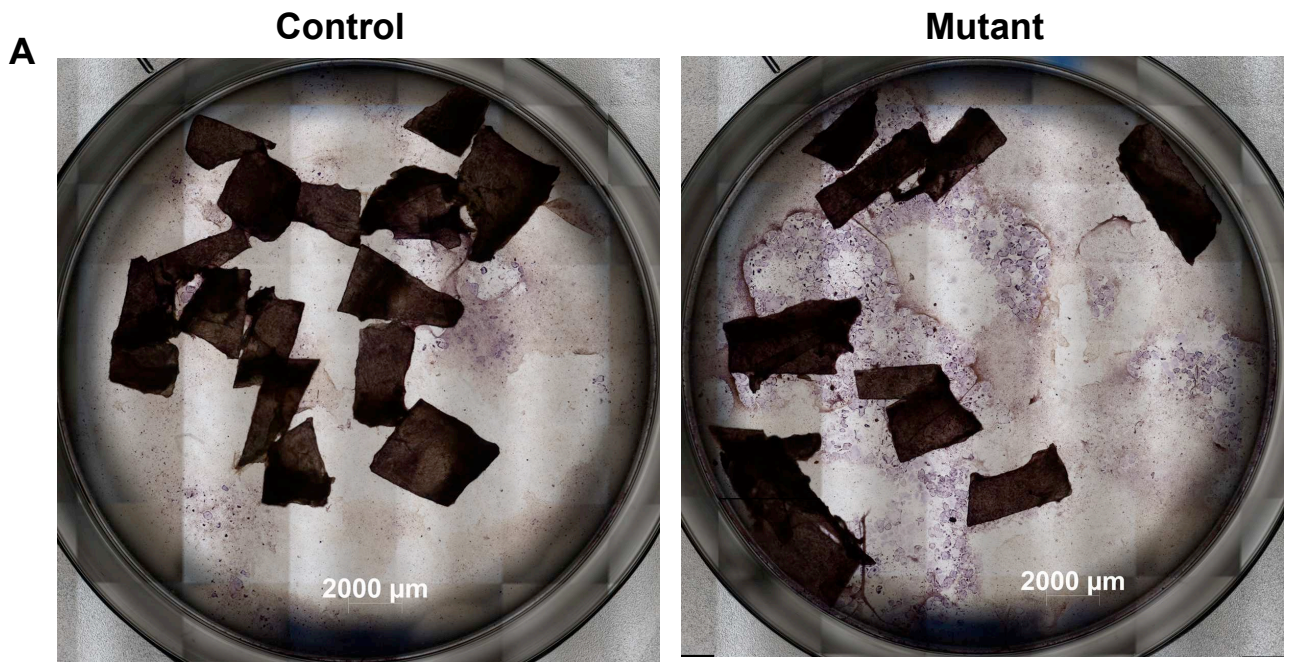
**A**





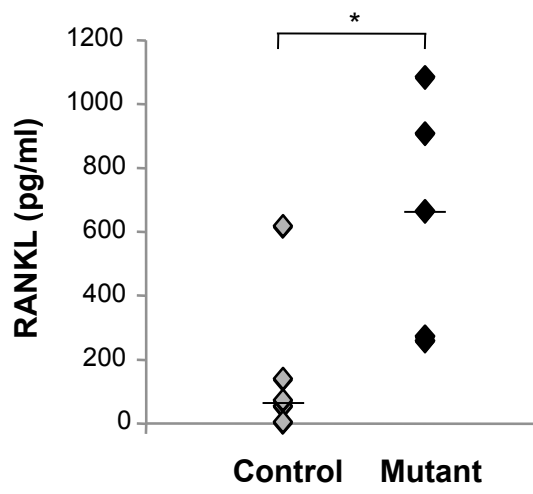


Nollet et al. Figure 4

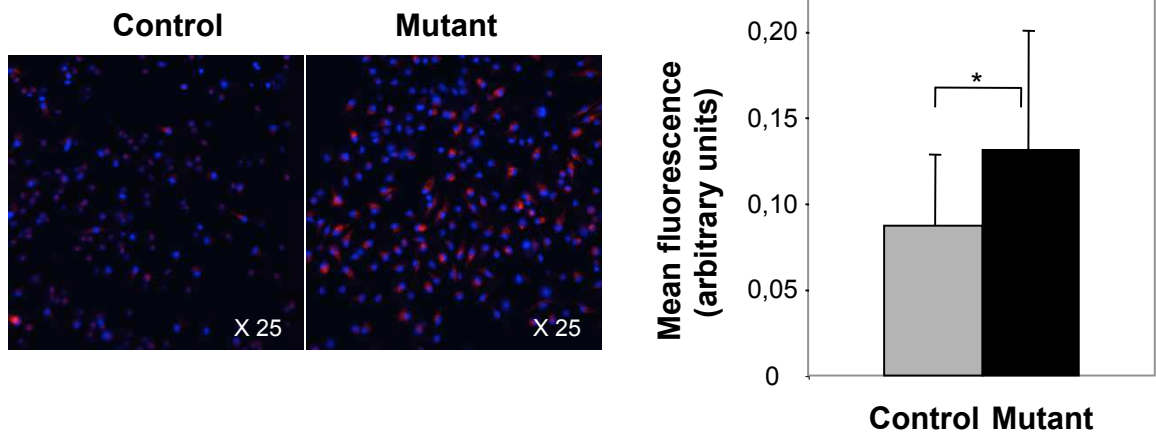


Nollet et al. Figure 5 A-B

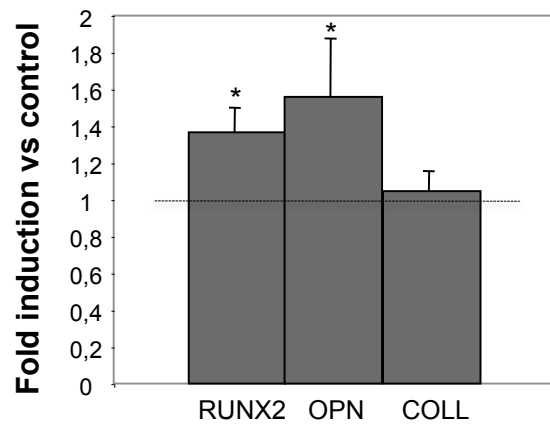
**C**

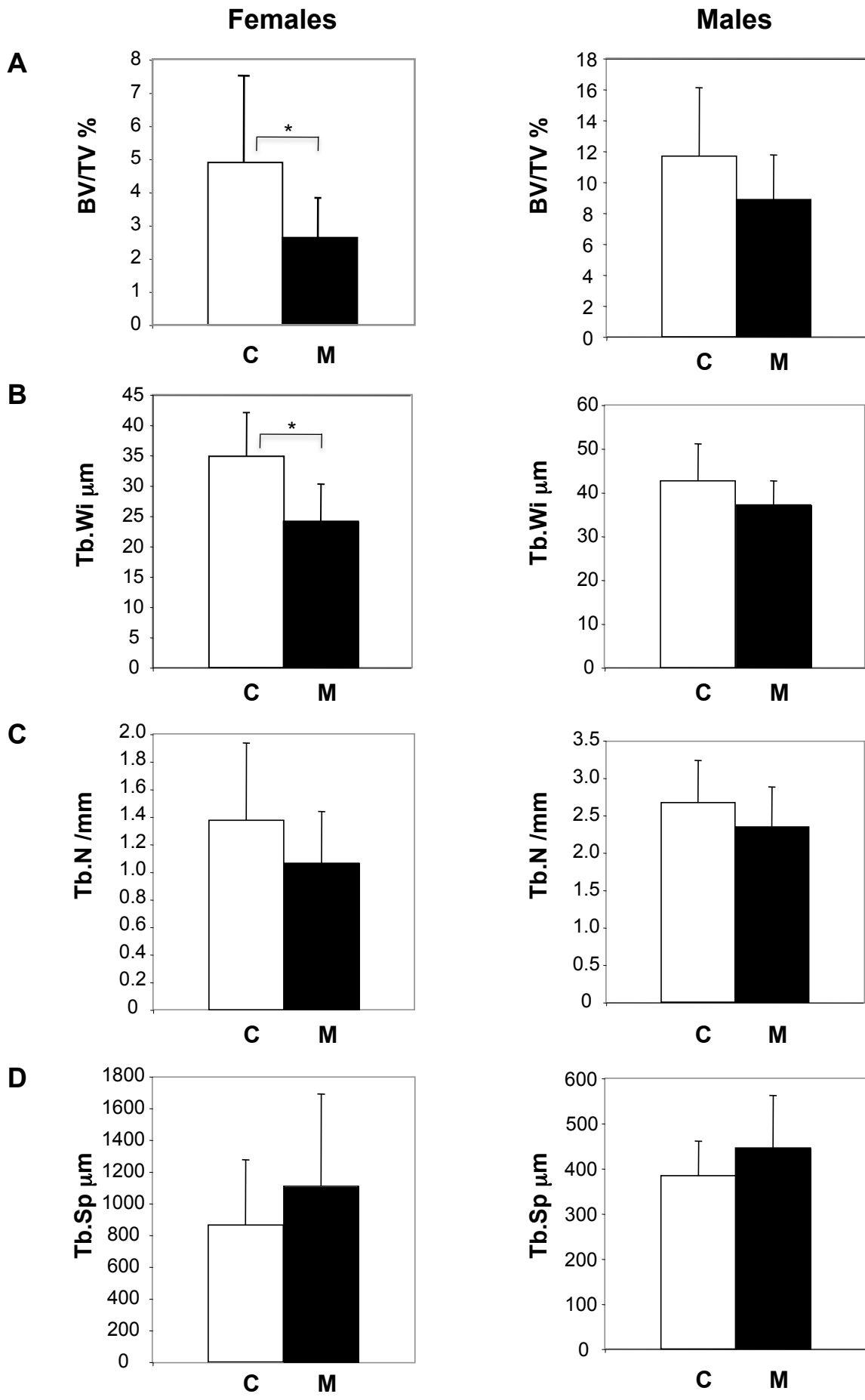


**D**

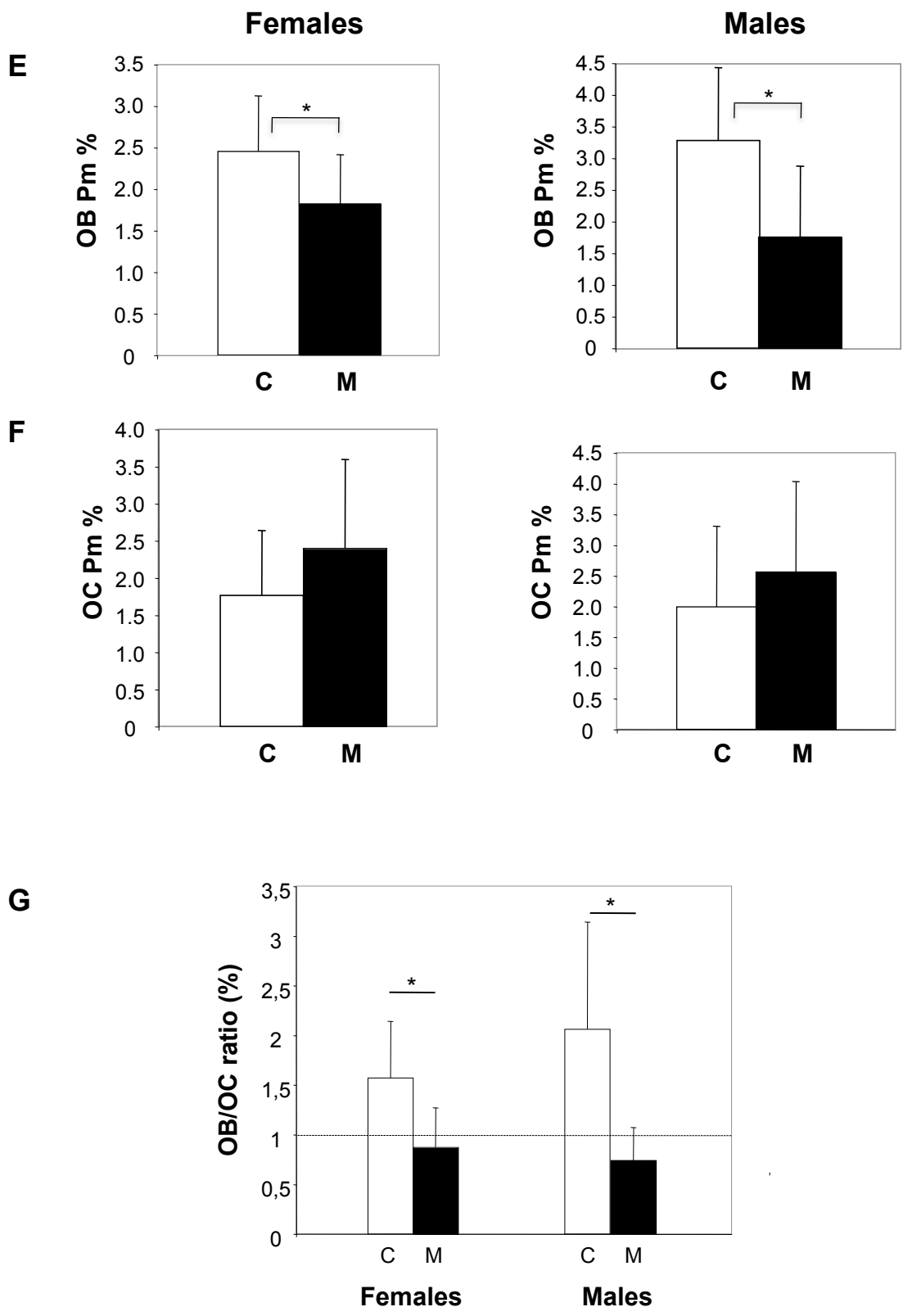


**E**





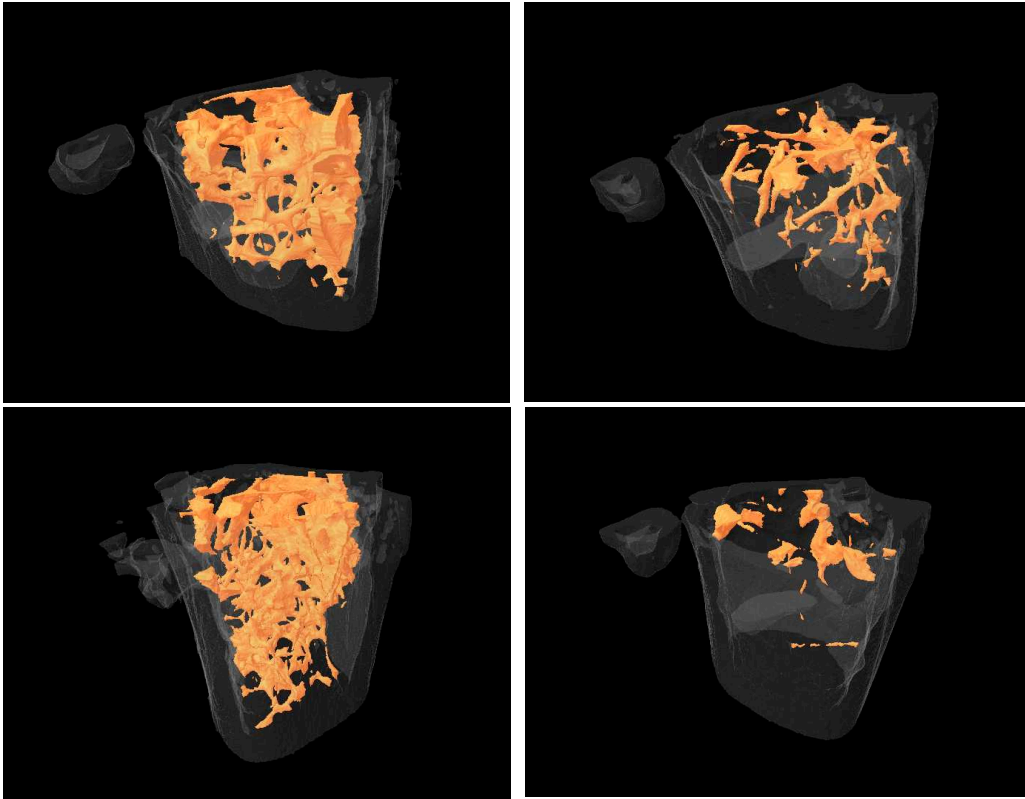
Nollet et al. Figure 6 A-F

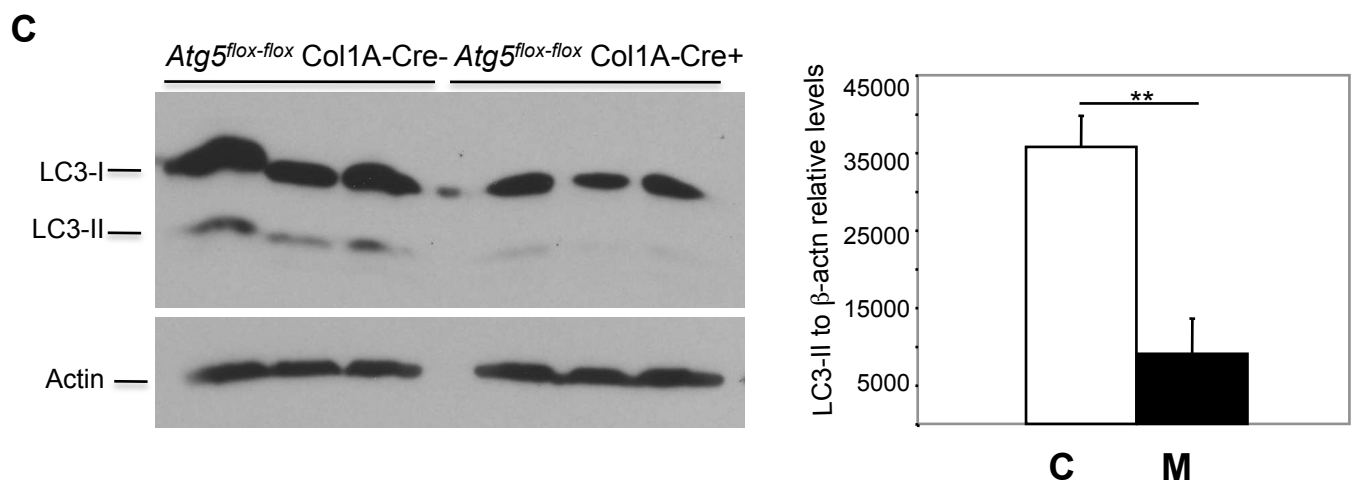
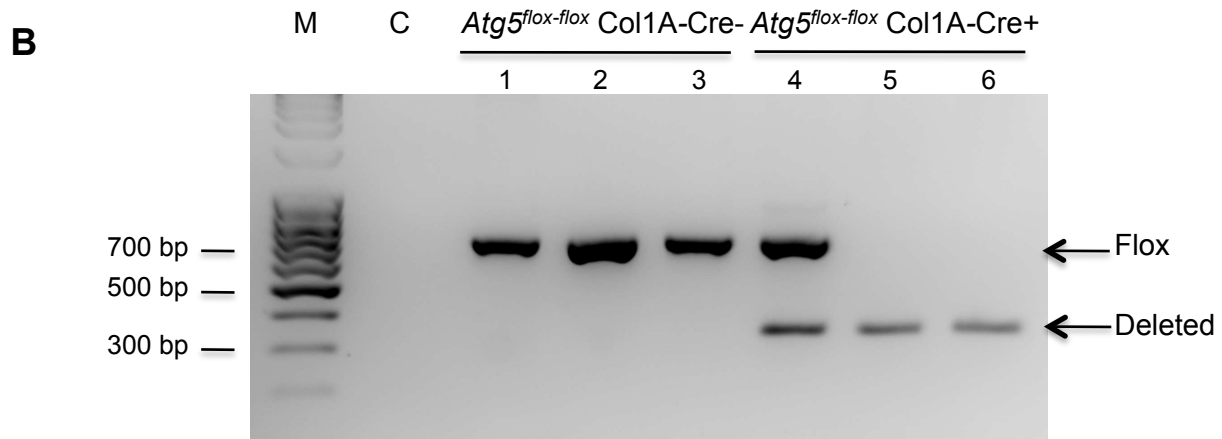
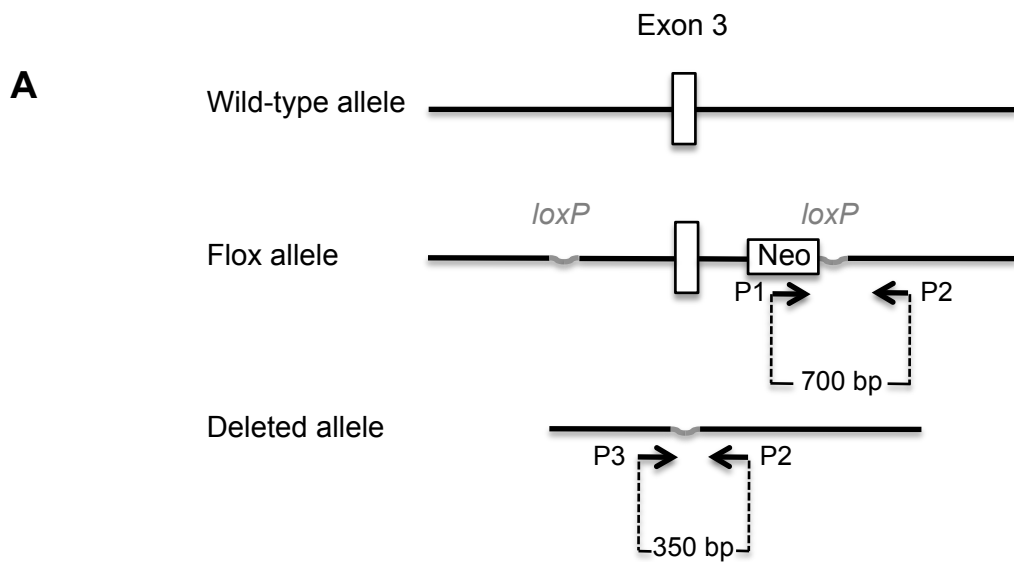


Nollet et al. Figure 6 A-G

**Control**

**Mutant**

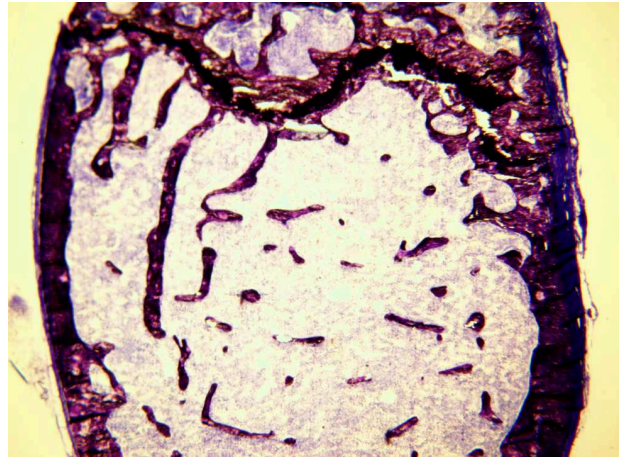
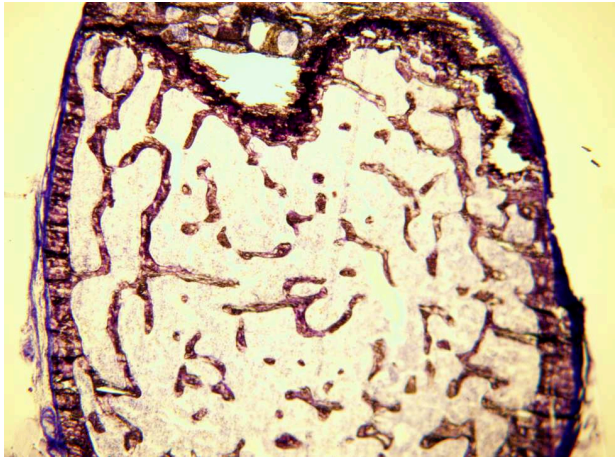




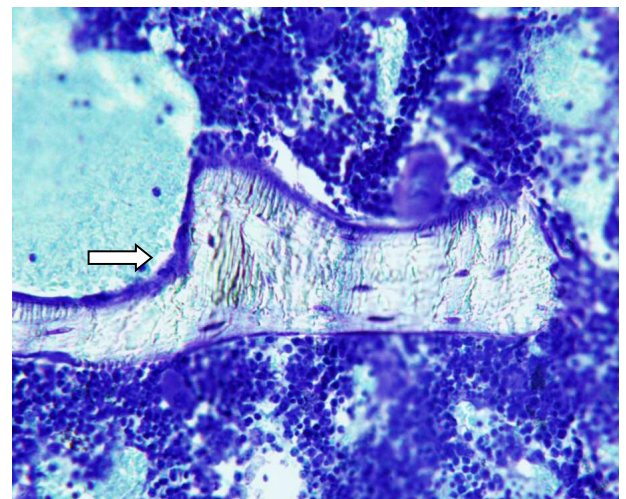
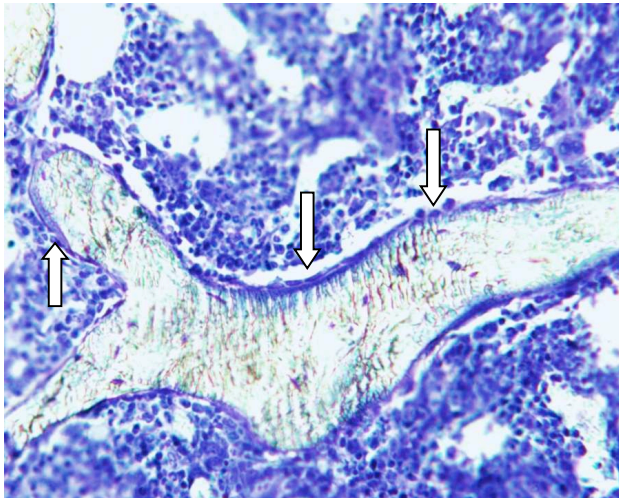
Control

Mutant

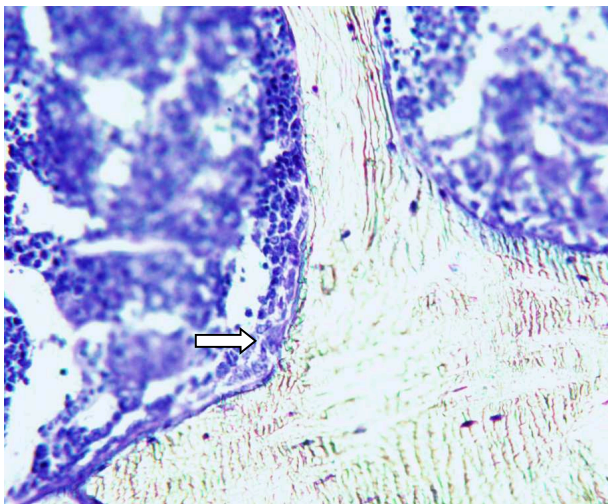
A



B



C



<b>Genotype</b> <b>Tb.Pf (1/<math>\mu</math>m)</b>	<b>BV/TV (%)</b>	<b>i.S (<math>\mu</math>m<sup>2</sup>)</b>	<b>Tb.N (1/<math>\mu</math>m)</b>
Control females (n=8) 18.25 $\pm$ 8.9	12.93 $\pm$ 7.1	2.18 $\pm$ 0.9	1.48 $\pm$ 0.7
Mutant females (n=9) 27.08 $\pm$ 5.7*	5.58 $\pm$ 3.3*	0.83 $\pm$ 0.4*	0.69 $\pm$ 0.4*
Control males (n=9) 10.29 $\pm$ 3.8	22.60 $\pm$ 4.8	2.94 $\pm$ 0.5	2.72 $\pm$ 0.5
Mutant males (n=9) 12.90 $\pm$ 8.2	20.77 $\pm$ 10.8	2.49 $\pm$ 1.2	2.47 $\pm$ 1.0

**Table 1. Microcomputerized tomography of femur from female and male nine-month-old mutant *Atg5<sup>flox-flox</sup> Col1A-Cre+* mice and their control littermates.** Values indicate mean  $\pm$  SD. BV/TV: Percentage of bone volume per total volume; i.S: Intersection surface; Tb.N: Trabecular number per  $\mu$ m; Tb.Pf: Trabecular pattern factor per  $\mu$ m. \*p < 0.05 vs control by Student's t test.